EVALUATING FACIAL ONTOGENY OF AVIAN EMBRYOS USING 3D GEOMETRIC MORPHOMETRICS

by

JOHNATHAN WOO

B.H.Sc., McMaster University, 2006

D.D.S., University of Toronto, 2010

A THESIS SUBMITTED IN PARTIAL FULFILLMENT OF

THE REQUIREMENTS FOR THE DEGREE OF

MASTER OF SCIENCE

in

THE FACULTY OF GRADUATE AND POSTDOCTORAL STUDIES

(Craniofacial Science)

THE UNIVERSITY OF BRITISH COLUMBIA

(Vancouver)

August 2014

Abstract

Objectives: In order to study abnormal facial development, reference standards of normal development are required. It is challenging to obtain 3D data on early embryos, since they are comprised of non-differentiated tissue. We used optical projection tomography (OPT) (Bioptonics, UK), which images transparent specimens with UV light. Here we used carefully staged chicken embryos to measure facial morphogenesis over time.

Methods: Chicken eggs (n=32) were incubated for 3.5-6 days (stage 20, 24, 28, 29). Embryo heads were fixed in formaldehyde, embedded in agarose, dehydrated in methanol, and then cleared in Benzyl Alcohol Benzyl Benzoate. Embryos were scanned with the OPT, images were reconstructed, and then the head was digitally resliced in the frontal plane using NRecon and CTan. Resliced files were imported into Amira, facial prominences were outlined, and isosurfaces were created. Volumetric measurements were assessed using Amira. Landmarks were applied to the surface of each prominence using Landmark. These landmarks were then superimposed from different embryos using MorphoJ, whereby they underwent Procrustes superimposition, Principal Component Analysis, Canonical Variate Analysis, and Discriminant Function Analysis.

Results: Traditional morphometrics revealed that the greatest amount of growth was a 24-fold difference in volume of the lateral nasal prominence between stages 20 and 29, followed by the maxillary, mandibular, and frontonasal mass. Geometric morphometrics revealed that embryonic facial prominences had minimal changes in shape between stages 20 and 24, however, after this time, there was more separation of the data in morphospace. Strikingly, the greatest morphological change was between stages 28 and 29, which was only 12 hours apart. This rapid change suggests that other mechanisms in addition to cell proliferation are involved. In addition,

the data show that major morphological changes precede lip fusion. Therefore, we can pinpoint our studies to stage 28, when critical events in the mesenchyme are taking place.

Conclusion: Embryonic chicken facial prominences undergo major shape changes. Each prominence varies in morphology with respective stage, with the frontonasal mass and mandibular prominence having the most dynamic shape changes.

Preface

Contributions of supervisor and student:

- Identification and design of the research program, 60% supervisor /40 % student
- Performance of various parts of the research, 100% student
- Analysis of the research data. 100% student

UBC Ethics Board

Fertilized white Leghorn chicken eggs were purchased from the University of Alberta .

The work was carried out under UBC animal ethics protocol A11-0351

Funding was obtained from the Faculty of Dentistry and CIHR operating grants to JMR.

Table of Contents

List of Tables

List of Figures

List of Abbreviations

BABB – Benzyl alcohol, Benzyl benzoate

CCD – Charged couple device

CVA – Canonical Variate Analysis

CV1 – Canonical variate 1

CV2 – Canonical variate 2

DFA – Discriminant Function Analysis

FNM – frontonasal mass

GFP1 – Green fluorescent protein 1 channel

GMM – geometric morphometrics

LNP – lateral nasal prominence

MD – mandibular prominence

MXP – maxillary prominence

OPT – optical projection tomography

PBS – Phosphate buffered solution

PCA – Principal Component Analysis

PC1 – Principal component 1

PC2 – Principal component 2

PS – Procrustes superimposition

TMM – traditional morphometrics

Acknowledgements

I would like to offer my sincerest thanks to Dr. Joy Richman for all her help and support over the past three years. Without her, I would not have been able to complete this project.

Many thanks to my committee members, Dr. Nancy Ford and Dr. Virginia Diewert for their support and guidance. I would also like to express my gratitude to my external examiner, Dr. Nathan Young of UCSF for assisting me with the revision of this thesis.

Thanks to the members of the Richman lab and especially to Theresa Grieco for her invaluable help with MorphoJ and understanding of GMM. Thanks to the Centre for High-Throughput Phenogenomics who provided the OPT scanner and Amira software for my analysis .

Special thanks are owed to my fiancée, sister, and parents, who have supported me throughout my countless years of education. Thank you for all your love and support.

Chapter 1: Introduction

1.1. Review of chicken craniofacial development

In order to study the natural development of the facial prominences of the embryonic face, reference standards are required to determine the dimensional and volumetric changes seen in these structures. The chicken embryo is ideal for these experiments due to the ease in accessibility, and ability to induce reproducible changes to facial morphogenesis. The embryonic face passes through distinct phases of development beginning with the formation of neural crest cells, to the ventral migration of these cells, and then to the formation of the facial prominences. Neural crest cells migrate from the dorsal neural tube to form the majority of the mesenchymal tissue of the facial prominences (Chai et al., 2000; Couly et al., 1993; Minoux and Rijli, 2010). The information for skeletal size is contained in the neural crest cells as shown in quail-duck grafting experiments (Fish et al., 2014; Hall et al., 2014; Schneider and Helms, 2003). Outgrowths from the first pharyngeal arch and the upper face, ventral to the forebrain, give rise to the individual facial prominences. The prominences are buds of neural crest-derived mesenchyme covered in epithelium that grow around the nasal pits and oral cavity. The facial prominences consist of the frontonasal mass, the paired lateral nasal prominences, and the paired maxillary and mandibular prominences. The frontonasal mass is medial to the nasal pits, while the lateral nasal prominences are lateral to the nasal pits. The frontonasal mass and lateral nasal prominences grow out and fuse with the maxillary prominences to form the upper lip or beak in the bird. The entire lower beak is formed by the mandibular prominences. Detailed fate mapping of the prominences determined that the frontonasal mass gives rise to the midline including the nasal septum, premaxillary bone, prenasal cartilage and the egg tooth (Richman and Tickle,

1989; Richman and Tickle, 1992; Wedden, 1987). The lateral nasal prominences form the nasal turbinates (MacDonald et al., 2004). The maxillary prominence outgrowth enlarges and extends below the eye and forms the lateral aspect of the stomodeum. As the maxillary prominence enlarges, they fuse with the frontonasal mass and lateral nasal prominence to form the structure of the upper; including the sides of the upper beak, tip of the beak and the palate (Lee et al., 2004). The inferior mandibular prominences contain the paired Meckel's cartilage, and form the dentary, and other bones of the lower beak (Richman et al., 1997; Richman and Tickle, 1989; Richman and Tickle, 1992).

Reciprocal epithelial-mesenchymal signaling is required for outgrowth. Initially signals from the brain (Marcucio et al., 2011; Young et al., 2010; Young et al., 2014) and foregut (Benouaiche et al., 2008; Brito et al., 2006; Couly et al., 2002) influence where the jaws will form in the head. Later, when facial prominences are established, the epithelium and mesenchyme each play a role in forming the correct arrangement of bones in the face. When epithelium is removed, growth of the skeletal elements is inhibited. For example cartilages derived from the mandibular or frontonasal mass prominences are severely stunted when epithelium is stripped off (MacDonald et al., 2004; Richman et al., 1997; Richman and Tickle, 1989; Richman and Tickle, 1992). The final shapes of the facial prominences appear to be derived from mesenchyme, and not epithelium as shown in recombination experiments where epithelium and mesenchyme was exchanged between facial prominences (Richman and Crosby, 1990; Richman and Tickle, 1989; Richman and Tickle, 1992; Wedden, 1987). Facial prominence growth at later stages is somewhat autonomous and does not depend on the rest of the head. Individual prominences can be grown outside of the face when grafted to an ectopic location such as the limb bud (Wedden, 1987).

One of the most important outcomes of embryonic facial development is the correct fusion of the upper facial prominences to form the lip. The two main developmental processes that bring the individual facial prominences together are fusion and merging(Johnston and Bronsky, 1995). Fusion occurs when two epithelial-lined structures contact and create a bilayered epithelial seam. This seam is later removed by a combination of apoptosis, epithelial-mesenchymal cell transformation, and cell migration to adjacent epithelium (Shuler, 1995; Sun et al., 2000). Fusion occurs between the frontonasal mass, lateral nasal prominence and maxillary prominence, as well as in the midline of the palate (Sun et al., 2000). In chickens, palatine processes develop but remain unfused, resulting in a natural cleft (Abramyan et al., 2014; Richman et al., 2006; Young et al., 2014). Merging involves filling in of a groove between partially attached developmental structures via migration and proliferation of underlying mesenchymal cells. Merging occurs between the lateral nasal prominence and maxillary prominence and in the midline of the mandibular prominence.

Another important aspect of facial morphogenesis is the narrowing of the face which results in the eyes moving closer together towards the midline. In the case of the human, the eyes start out on the side of the head just as in other animals but then they migrate to the front of the face. The narrowing of the frontonasal region is associated with forming a defined midline in the face across which features are symmetrically arranged. The basis for actual facial narrowing is poorly understood and could be either due to an actual narrowing of the frontonasal mass or relative narrowing in relation to the rest of the head growing. For example the rate of growth of the frontonasal mass may be less than the surrounding lateral nasal prominences and eyes which makes it appear as though the frontonasal mass is narrowing. Intrinsic narrowing is due to shape changes within the frontonasal mass itself. Such shape changes could begin with the

mesenchymal cells actively moving or being displaced towards the centre. Such movements may make the prominences elongate in one axis and narrow in the perpendicular axis. This morphogenetic process is called convergent extension (Wallingford et al., 2002) and has not yet been measured in the facial development of any animal. The two processes, convergent extension and lip fusion are most likely interrelated. For example, convergent extension may bring the frontonasal mass and maxillary prominence closer together so that they may fuse.

Many craniofacial abnormalities include widening or excessive narrowing of the facial midline. One notable midline characteristic is the varied distance between your eyes. Hypertelorism is an abnormal increase in intraorbital distance, while hypotelorism is an abnormal decrease in intraorbital distance. These abnormalities can occur as a morphogenetic variant, a primary deformity, or a secondary phenomenon in association with developmental abnormalities (DeMyer, 1975; Diewert and Lozanoff, 1993b; Dubourg et al., 2007; Muenke and Beachy, 2000; Muenke et al., 2010; Vermeij-Keers et al., 1984). Median cleft face syndrome is a condition associated with hypertelorism and median plane facial anomalies with normal to minimal developmental delay and a normal prognosis for survival(Vermeij-Keers et al., 1984). In contrast, holoprosencephaly or cylcopia are at the end of the spectrum for hypotelorism. The holoprosencephaly phenotype consists of median cleft lip, single central incisor, narrow or deficient nose, and structural brain abnormalities associated with gross developmental delay and poor prognosis(Belloni et al., 1996; Muenke and Beachy, 2000; Muenke et al., 2010; Roessler et al., 1996).

1.2. Shaping the face, proliferation and morphogenesis of facial prominences

During embryogenesis, the facial prominences grow in a highly choreographed manner to achieve its final shape. In the chick embryo, cell proliferation has also been studied in different regions of the face and correlations have been made to the direction of growth. Proliferation rates of facial mesenchyme are generally high at young stages such as stage 20, and decline gradually until stage 29 (Abramyan et al., 2014; Bailey et al., 1988; Minkoff and Kuntz, 1977; Minkoff and Kuntz, 1978). Within the frontonasal mass, highest proliferation indices are measured in the areas adjacent to the nasal processes (Bailey et al., 1988; Minkoff and Kuntz, 1977; Minkoff and Kuntz, 1978). The centre of the frontonasal mass has relatively low proliferation especially at stage 28 when the prenasal cartilage begins to differentiate (MacDonald et al., 2004; McGonnell et al., 1998; Szabo-Rogers et al., 2008). In the lateral nasal prominence, distal cell proliferation accounts for expansion along the mediolateral axis, and those that border the nasal pits accounts for most expansion (McGonnell et al., 1998). The anterior half of the maxillary prominence (superior half) elongates and broadens between stage 24 and 28, more so than the posterior half (inferior half) (McGonnell et al., 1998). In the maxillary and mandibular prominence, there is also increased proliferation along the proximodistal axis leading to outgrowth at their tips (Barlow and Francis-West, 1997; McGonnell et al., 1998).

Cell proliferations accounts for the growth of tissue; however, there are several theories into how the final tissue shape is achieved. In round tissues such as the early maxillary prominence, cells may simply expand equally in all directions (Bailey et al., 1988). In tissues with unique shapes and outgrowths like the frontonasal mass and mandibular prominence, the mechanism is not as simple and may involve a balance between proliferation, cellular movement (McGonnell et al., 1998; Patterson and Minkoff, 1985), apoptosis (Ashique et al., 2002a;

McGonnell et al., 1998), cell polarity (Li et al., 2013), and possibly even cell tension (McGonnell et al., 1998).

The most careful study on mesenchymal cell behavior in the face was carried out in the chicken embryo using DiI injections. Dye was injected at stage 20 and embryos were allowed to grow for 48h until they reached stage 28. Shapes of the dye spots were measured in 2D photographs of the head viewed from the front. Results revealed that cells situated around the nasal pits, the midline of the paired mandibular prominences, and areas of fusion between the frontonasal mass and maxillary prominence contribute most to expansion of the face (McGonnell et al., 1998). Many cell populations also display an axis of preferential expansion, and that medial and proximal cell populations contribute more to enlargement than lateral cell populations, and predominantly in the proximodistal axis (McGonnell et al., 1998). In the frontonasal mass, the distal cell populations expand mediolaterally, resulting in outgrowth at the base of the frontonasal mass. Orbital enlargement and medial growth of lateral nasal prominence also contributes to frontonasal mass development (Patterson and Minkoff, 1985). In contrast, in the maxillary prominence and mandibular prominence there seem to be regional differences in growth. The distal-most cell populations expand proximodistally, resulting in outgrowth at the tips (MacDonald et al., 2004; McGonnell et al., 1998). In addition, the anterior maxillary prominences expand more in the proximodistal direction than the posterior half (McGonnell et al., 1998). However in more detailed proliferation analyses between stage 24 and 29, the posterior end of the maxillary prominence maintains higher proliferation relative to the anterior mesenchyme (Abramyan et al., 2014). Lateral nasal prominence development appears to be a consequence of forebrain enlargement and lateral expansion of the edges of the frontonasal mass but much less is known about this region compared to the others.

At the molecular level, certain growth factor signaling in the facial prominences affects final beak size and shape. Many studies have been carried out on chicken embryos in which levels of growth factors have been increased or their pathways blocked with antagonists. Increased levels of BMP (Bone Morphogenetic Protein) signaling can either induce (Barlow and Francis-West, 1997) or reduce proliferation and size of the facial prominences (Ashique et al., 2002a; Wu et al., 2006; Wu et al., 2004). The insertion of viruses expressing BMPs (Abzhanov et al., 2004; Hu et al., 2008; Wu et al., 2006; Wu et al., 2004) or their receptors (Ashique et al., 2002b) generally increases the size of the skeletal elements. Noggin, the BMP antagonist, inhibits proliferation of the maxillary prominence and leads to clefting in the chicken embryo (Ashique et al., 2002a). Overexpression of Noggin using a retrovirus leads to miniaturized beaks (Abzhanov et al., 2007; Foppiano et al., 2007; Hu et al., 2008; Wu et al., 2006; Wu et al., 2004). Sonic Hedgehog (SHH) regulates brain width and signals to the frontonasal mass epithelium to increase proliferation of the underlying mesenchyme. SHH in the epithelium at the edge of the frontonasal mass is important for setting up the width of the face (Cordero et al., 2004; Marcucio et al., 2011; Young et al., 2010; Young et al., 2014). Fibroblast growth factors (FGF) are required for lateral nasal (Szabo-Rogers et al., 2009) and frontonasal mass growth (Szabo-Rogers et al., 2008). Blocking FGF signaling with a bead soaked in an antagonist induced facial clefting, and deletion of the lateral edge of the premaxillary bone (Szabo-Rogers et al., 2008). The expression of Wingless-related genes in the facial prominences also implies that they control shaping of the facial prominences. Indeed overexpression of WNT5A in the mandible leads to a smaller beak on the injected side and lower proliferation (Hosseini-Farahabadi et al., 2013). In addition to individual effects of growth factors, the various pathways also intersect each other. For example FGFs and BMPs both induce Muscle-specific homeobox (MSX) transcription

factors. In addition, growth factors may also regulate expression of other factors. For example FGF2-soaked beads inhibit expression of BMP4 (Szabo-Rogers et al., 2008). Thus any disruption in balance of signaling pathway activity could lead to changes in shape or size of the facial prominence. Slight alterations in signaling could lead to the variations in normal face shape seen within a population or could contribute to species-specific facial morphology (Young et al., 2010; Young et al., 2014). More significant disruptions in signaling could result in facial deformities such as orofacial clefts, hypo or hypertelorism or mandibular dysplasia.

1.3. 3D imaging methods

Vertebrate embryo development is a complex and dynamic process that involves growth and deformation in 3D, however it is hard to capture the changes in a quantitative manner. Preexisting techniques for imaging whole embryos involved embedding the embryo in wax and physically sectioning them via microtome. The next step was to photograph the sections, align and stack the photographs and finally to go through the stack of images and outline areas of interest (Diewert and Lozanoff, 1993b; Ooë, 1981; Radlanski, 2003; Radlanski et al., 2003). WinSURF Reconstruction Software was developed at the University of British Columbia and the University of Hawaii to carry out 3D reconstructions from individual sections (Aldur, 2005; Landes et al., 2006). Unfortunately, compression of the wax during sectioning introduces variation in between the sections. This makes it difficult to skip sections during the alignment since there are quite large differences from one section to the next. Various attempts to add objects into the wax block to assist with alignment have been tried but these did not completely resolve the problems with reconstructing a whole object from paraffin sections. Block face imaging is a similar technique, but instead of sectioning first, an image is taken of the "block

face" just prior to cutting. This allowed for better shape preservation, though, some compression and deformation was still applied to the original specimen (Mohun and Weninger, 2011; Weninger and Mohun, 2002). Ultimately the tissue reconstruction process is time consuming, and technique sensitive.

The invention of nondestructive medical imaging techniques has made it possible to have perfect alignment of slices since they are taken from a whole object. Nondestructive imaging generate images from living or fixed embryos using gamma rays, electron beams, lasers, light and x-rays. The methods include microMRI (magnetic resonance imaging), microCT (computerized tomography) and microscopic ultrasound imaging. As these beams and rays do not deflect as they pass through a specimen, projection tomography collects data from a sum of linear projections that pass through the specimen, and transform the data with a filtered back projection algorithm to recreate the image. The specimens are sampled at discrete points in space which are then mapped to a voxel for the reconstruction.

Each method has advantages and disadvantages. Micro CT has a resolution of 10 microns or less and can be used even for non-mineralized embryos (Beckmann et al., 1997; Bonse and Busch, 1996; Metscher, 2011; Metscher and Muller, 2011). The technique is best suited for ossified tissues where there are clear differences between radiodense and less dense tissues (Metscher, 2011; Metscher and Muller, 2011).

MicroMRI will reveal soft tissue architecture without the need for adding contrast agents. However it is very expensive, and has poor resolution (25 micrometers), making it unsuitable for identifying internal structures within an embryo (Jacobs et al., 1999; Louie et al., 2000; Schneider et al., 2003).

Microscopic ultrasound imaging requires little tissue preparation and could be quite convenient since penetrance is quite good. However ultrasound suffers from poor resolution (50 micrometer) (Foster et al., 2011; Stiebel-Kalish et al., 1997; van Raaij et al., 2011).

Optical coherence tomography uses optical scattering and reflectiveness to generate 3D images, but can only penetrate 2-3mm, and is also unable to scan an intact specimen (Gu et al., 2011; Larina et al., 2011)

Optical projection tomography (OPT) is a relatively new 3D imaging technique that was developed to fill in this gap in imaging technology for small specimens. OPT scans can cover whole specimens (1-15mm in diameter) at high resolution (<10 micrometer) (Sharpe, 2003; Sharpe, 2004; Sharpe et al., 2002). The OPT projections can be reconstructed and visualized as 3D iso surfaces. Moreover in the slices through the reconstructed specimen, the differences in density of internal structures such as cartilages and muscles can be observed.

The cleared specimen is first suspended in an index-matching liquid to reduce scattering of the light, and to reduce any discrepancies of refractive index through the specimen (Quintana and Sharpe, 2011a; Quintana and Sharpe, 2011b). This allows for the light to pass through the specimen in a relatively straight line. As the transparent embryo is rotated through 360º through a series of angular positions, an image is captured at each orientation. The axis of rotation is aligned perpendicular to the optical axis so that the projection data of each plane is collected by a linear row of pixels on the sensor. The light can be ultraviolet, white or infrared thereby allowing detection of fluorescent probes or chromogenically stained tissues. The instrument records the light that passes through the object. Lenses focus this image onto a charged couple device sensor, and through a back projection algorithm within the OPT software, the original 3D information is reconstructed (Quintana and Sharpe, 2011a; Sharpe, 2003; Sharpe, 2004; Sharpe et al., 2002).

Many of OPTs advantages derive from it being an optical technique. Precise shape and structure can be conserved without having to dissect it away from its neighbouring tissue. It is suited for specimens 1-15millimetres in maximum width, as it is limited due to the size of the loading cuvette. The resolution of OPT also depends on the size and type of specimen, but it is typical to reconstruct at <10 micrometers.

The OPT overcomes a disadvantage of microscopy where depth of focus is limited (Quintana and Sharpe, 2011a; Sharpe, 2004; Walls et al., 2005). With large specimens, the depth of focus may not be large enough to pass through the entire specimen. Points further from the focal plane will not appear sharply focused, while points closer to the plane will appear focused. Instead of having to scan the specimen at multiple depths, the OPT accommodates by positioning the focal plane halfway between the axis of rotation and the edge of the specimen closest to the lens. This ensures that the entire specimen is imaged in focus for the full 360º rotation. Of course, the higher the zoom, the more difficult it will be to keep all of the specimen in focus.

A disadvantage of the OPT is that native fluorescent signals such as those from Green Fluorescent protein are not preserved during the processing. In order to make these signals visible it is first necessary to immerse the fixed embryo in the antibody to the protein of interest and then to detect the antibody with a fluorescent tag. The wholemount immunofluorescence method adds complications to the procedure and may not work for all antibodies. I will be using OPT imaging for my study on embryonic facial morphogenesis but will not be using antibody staining as part of the procedure. Instead I will rely on the natural autofluorescence of aldehyde-fixed tissues.

1.4. Morphometrics

To measure the shape of the face I will be using a measurement method called morphometrics. The history of morphometrics goes back more than 100 years. Albrecht Dürer's early attempts at studying human proportions by transforming faces to a coordinate grid influenced and inspired D'Arcy Thompson's classic 'On Growth and Form' (Figure 1)(Dürer, 1525; Thompson, 1917). Thompson found that related species superficially looking very different could in some cases be represented as simple Cartesian transformations of one another (Thompson, 1917). Modern morphometrics was driven by Fred Bookstein (Bookstein, 1991). He attempted to explain Thompson's graphical technique by formalizing the mathematical calculations, known later as 'bioorthogonal analysis'(Bookstein, 1991). This analysis was later termed geometric morphometrics, which is a sophisticated, quantitative measurement of the variation in organismal size and shape using multivariate statistics. Quantitative morphogenesis was ultimately applied to embryos. One of the early pioneers was Dr. Virginia Diewert at UBC. Diewert and Lozanoff in 1993 (Diewert and Lozanoff, 1993b) looked into human primary palate and midface formation (Diewert and Lozanoff, 1993a), and determined the direction and quantity of development in 3D through the reconstruction of histological sections and Fourier transformation.

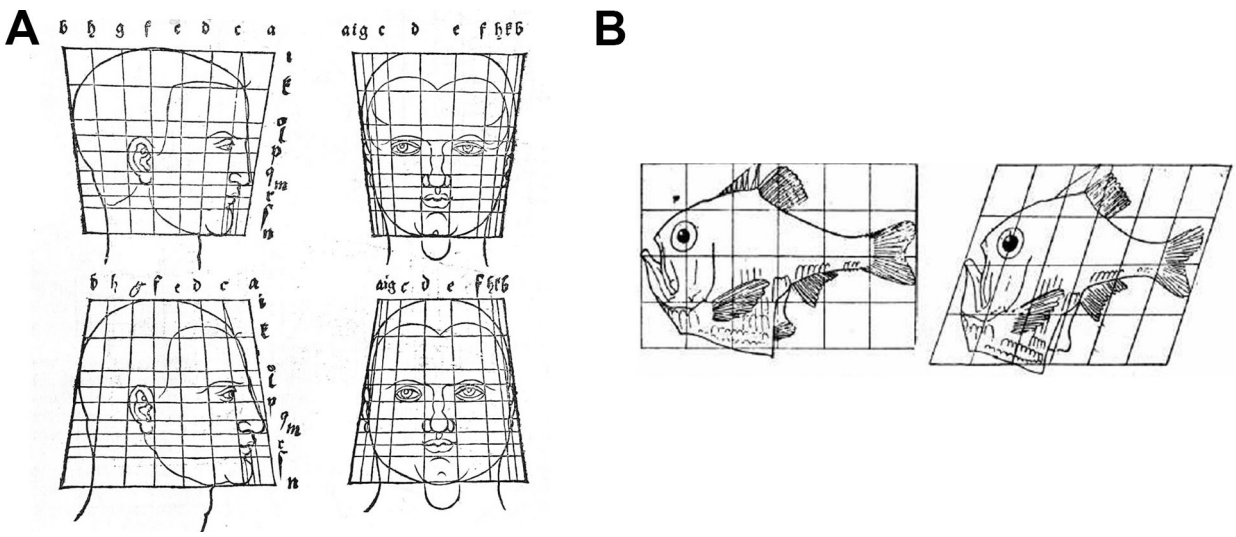

Figure 1 – Dürer and Thompson's work
A – Dürer's study of human proportions, and the use of transformations to a coordinate grid to demonstrate facial variations. B –Hand-drawn transformation, with a 70° linear shear of *Argyropelecus olfersi (left)* into his cousin *Sternoptyx diaphana (right)* from D'Arcy Thompson's 1917 classic On Growth and Form.

There are two major types of quantitative morphometrics: traditional morphometrics (TMM) and geometric morphometrics (GMM)(Zelditch et al., 2012). TMM involve linear distances (ie. length, width, height), angles, areas, and volumes. They are simple measurements, and are highly correlated with size. These measurements are useful especially over a developmental series but do not capture shape differences. GMM is the quantitative representation and analysis of morphological shape using geometric coordinates instead of measurements (Zelditch et al., 2012).

To perform GMM, it is necessary to locate the specimen surface in 3D space. Either meshes or landmarks can be used to define the surfaces. Landmarks are coordinate points described with Cartesian coordinates (x,y,z in 3D space) that are used to describe the shape of a

structure. Landmarks can be points on a biological or geometrically homologous point on the structure. Semi-landmarks are points that are placed arbitrarily, usually between biological homologous points. Outlines are perimeters defined by numerous points. Surfaces involve the 3D surface of an object. They are also both described using Cartesian coordinates (x,y,z), and numerous points comprise a mesh that covers the surface of the object. Landmarks, outlines and surfaces must be present in all subjects, and must represent the shape of the object adequately.

GMM relies on multivariate statistics for the quantitative analysis of overall shape. Multivariate statistics are necessary when more than one variable is to be compared, and are not completely independent of each other. Results in GMM are presented visually as a shape, rather than tables and numbers in TMM. In TMM, the size of the object affects all measurements, and the only identifiable differences within a group are size, rather than shape. GMM allows for quantification of subtle differences in shape that may be present on a continuum, and may not be apparent through other analysis (Klingenberg, 2010). GMM removes size by translating, rescaling, and rotating objects. Examples include Procrustes superimposition (PS), Euclidean Distance Matrix Analysis (EDMA), Principal Component Analysis (PCA), Canonical Variate Analysis (CVA), and Discriminant Function analysis (DFA). However GMM does not fully account for size heterogeneity that may exist in a sample. In order to remove the allometric component it is necessary to use the residuals of a multivariate regression on size to make statistically valid comparisons.

PS aligns shapes, and minimizes differences between them to ensure that only real shape differences are measured (Zelditch et al., 2012). The three steps in PS involve centering all shapes to an origin, scaling all shapes to the same size, and rotating each shape around the origin until the sum of squared distances between the corresponding landmarks are minimized. There

are two types of PS: full, and partial. A full Procrustes fit accounts for scaling, while a partial Procrustes fit does not rescale (ie. the size of the object is preserved). With a full Procrustes fit, if their shape is identical, the objects will match, but in a partial Procrustes fit, if their shapes are identical, and their sizes are different, the objects will not match. PS translates the centroid of the shapes to (0,0,0), whereby the x,y,z coordinates of the centroid is the mean (x,y,z) coordinates of all the landmarks.

EDMA is a morphometric analysis that uses landmark coordinate data without using a fixed coordinate axis. The analysis calculates all the linear distances between all possible pairs of landmarks in each individual and compares these distances as ratios between groups. This method has been previously used in human and nonhuman studies and is a widely accepted method for morphometric comparisons (Zelditch et al., 2012).

PCA can be used to examine the main features of shape variation in a sample, and as an ordination analysis for examining the arrangements of specimens in morphospace (Savriama and Klingenberg, 2011). PCA is a way to reduce data dimensionality. It projects the data in the least squares sense, captures big (principal) variability in the data, and ignores small variability (Zelditch et al., 2012). Variance is reapportioned into new explanatory variables (principal components) associated with axes that account for the greatest covariation. Data points are presented in a rotated orthogonal coordinate system, where the origin is the mean of the data points. Axes are provided by the eigenvectors, which represent the orthogonal directions of greatest variability (covariance) in the data. Eigenvalues show the significance of the corresponding axis, and how much of the variance is reapportioned to each one of the new explanatory variables (principal components).

CVA provides a different type of ordination analysis, which maximizes the separation of specified groups chosen by the investigator (Savriama and Klingenberg, 2011). CVA is a multivariate data reduction method designed to maximize the differences between two or more groups (Zelditch et al., 2012). DFA is conceptually similar to CVA but instead of including all of the samples, DFA compares between two specified groups.

I will be analyzing the face at several discrete timepoints during development and will use a combination of TMM and GMM to quantify dimensional changes over time.

1.5. Software for morphometric analysis

Multiple software programs are required to take 3D datasets to the form suitable for GMM. The OPT Scanner 3001 (Bioptonics, Edinburgh, United Kingdom) comes with a prepackaged OPT scanning software program (NRecon, Bruker Skyscan, Kontich, Belgium) which is responsible for interpreting and reconstructing the scanned images into a 3D model using a back-projection algorithm. Once reconstructed, files are imported into CTan (Bruker Skyscan, Kontich, Belgium) to be resliced into the desired plane and thresholded to improve the contrast within the scans.

Amira (FEI Visualization Sciences Group, Burlington, Massachusetts, USA) is a software platform available for 3D visualization, processing, and analysis. It is used for processing and analyzing data from an array of 2D and 3D imaging methods. Amira's features include the ability to create isosurfaces and multiple regions of interest or segmentations from the reconstructed 3D models. These segmentations can then undergo volumetric analysis and TMM. Landmarks can also be applied in Amira.

To progress on to GMM, landmarks need to be marked on the specimen. Landmark (Institute for Data Analysis and Visualization, Davis, California, USA) is a freeware program developed from the University of California Davis campus for analyzing, interpreting, and visualizing 3D shape data. Originally designed for paleontology research, the program is used primarily for landmark editing and placement on geometric specimens and exports the landmark points for use in GMM software. The landmarks are imported to an analysis package. Many scientists use the free software, MorphoJ (Apache, Manchester, United Kingdom). It provides a platform for a wide range of GMM analyses. Features include importing/exporting datasets, Procrustes fit, generating covariance matrices, principal component analysis, canonical variate analysis, and Discriminant function analysis. I chose to use Landmark and MorphoJ based on their functionality, cost, and reliability.

1.6. Hypotheses

1. I hypothesize that it will be possible to separate embryos according to facial prominence shape and that the groupings will correspond to stage of development.
2. The frontonasal mass grows by convergent extension whereas the other facial prominences do not.

1.7. Aims

1. To describe the morphogenesis of stage 20 to stage 29 chicken facial prominences in 3D using landmark-based geometric morphometrics.

2. To obtain reference standards for each stage that can be used as comparisons for studies where growth is perturbed.

Chapter 2: Methods

2.1. Animals

Fertilized White Leghorn chicken eggs were obtained from the University of Alberta and incubated at 38ºC to the appropriate stage (Hamburger and Hamilton, 1951). Newly laid eggs are generally at stage 4 or early gastrulation. Storing eggs at cool temperatures (12-14°C) maintains eggs at this early stage until they are placed in an incubator at 38°C. As the rate of development can be affected by a range of factors like temperature and delays between laying and incubation, upon windowing the eggs, we staged each embryo using a standardized staging system (Hamburger and Hamilton, 1951). Eggs were initially windowed at 50-55 hours and were staged by counting the number of somites. Total somite-counts are typically 25-26 for a stage 15 embryo (Hamburger and Hamilton, 1951). If an embryo was above this number it was left out of the incubator for several hours to delay development while other embryos of the right stages were left in the incubator. It takes 3 hours for a somite pair to be elaborated. The stages we were interested in were:

Stage 20 (70-72 hours) – defining feature: presence of smooth wing bud between somites 17-20.

Stage 24 (4 days) - defining feature: limb bud longer than wide

Stage 28 (5.5 days) - defining feature: 2nd digit longer than 3rd digit

Stage 29 (6 days) - defining feature: elbow is forming and can be seen by a bend in the anterior margin of the wing.

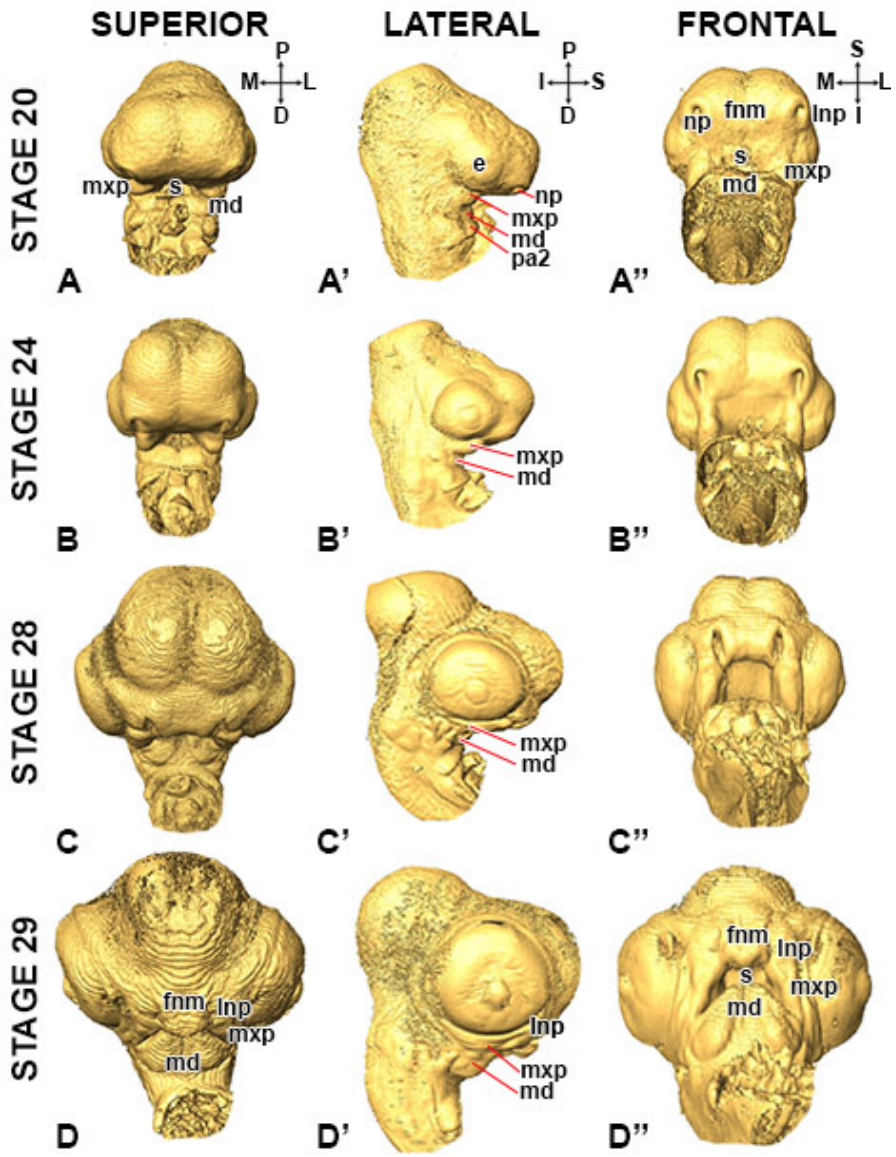

Figure 2 – Isosurfaces of the individual embryos at stage 20, 24, 28, and 29
Chick embryo heads are displayed in the superior, lateral, and frontal planes. Isosurfaces were created in Amira. For stage 20, the isosurface reconstruction used 1 in every 3 slices, while for stage 24, 28, and 29, the isosurface reconstruction used 1 in every 5 slices. This is visible as ridges on the surface of the embryo. Key: e – eye, fnm – frontonasal mass, lnp – lateral nasal prominence, md – mandibular prominence, mxp – maxillary prominence, np – nasal pit, s – stomodeum, pa2 – pharyngeal arch 2, pa3 – pharyngeal arch 3. Axes: D – distal, I – inferior, L – lateral, M – mesial, P – proximal, S - superior

2.2. Fixation, embedding and clearing for OPT scanning

Embryos were fixed in 10% buffered formaldehyde for several days or weeks. When it was time to embed into agarose for the OPT, embryos were rinsed extensively in Phosphate Buffered Saline (PBS) (0.02M phosphate, 0.15M NaCl), and cleaned of extra-embryonic membranes. Next a solution of 2% low melting point agarose made up in water was prepared in the microwave. The solution was poured into a crystallization dish and allowed to cool to approximately 42°C. Embryos were placed into the warm agarose and gently floated above the bottom and away from the sides of the dish as the agarose solidified. The agarose was then cut into blocks with the embedded embryo in preparation for OPT imaging. Each block was trimmed with a sharp blade to give a smooth surface, leaving 4-5 millimeters of agarose around the specimen.

The blocks were then dehydrated in 100% methanol over several days and cleared in a solution of BABB (1:2 benzyl alcohol to benzyl benzoate). This process replaces water (refractive index = 1.33) with BABB (refractive index = 1.56). As the specimen is also immersed in a solution of BABB when scanning, this helps eliminate optical scatter during OPT scanning. The high refractive index also helps to match the refractive index of the tissue.

2.3. Scanning and reconstruction of embryos in 3D

When ready to scan, each block was mounted to a magnetic stub using a cyanoacrylate adhesive. The stub was then mounted in the OPT Scanner 3001 (Bioptonics, Edinburgh, United Kingdom) so that the stub containing the embryo was inverted into a quartz cuvette containing BABB. The specimen was lowered into the cuvette by the SkyScan3001 software Version 1.3 (build 13). After centering the specimen, the UV light was turned on and exposure (200-800ms)

was adjusted for each specimen. Exposure times depended on the level of autofluorescence in each embryo and could vary also with the age of the embryo and the zoom factor used. The zoom was adjusted so that the embryo filled the field of view but did not swing out of the field in any of the rotational views. Exposure was adjusted so all parts of the embryo were in the middle of the range of intensities with no tissues being completely white or black. The autofluorescence was captured using the GFP1 filter (excited 425nm/40nm, emitter LP475nm).

During scanning, the specimen was rotated 360 degrees around its perpendicular axis stepwise every 0.9 degrees to completion. After each step, a still picture was taken (Figure 3A-D'). Images were captured using a #2 focusing lens, with pixel sizes ranging from 3 to 9 micrometers depending on whether high or standard resolution was used (512X512 is standard, 1024x1024 is high resolution). The 400 images were processed to generate 3D voxel information using NRecon software, and then resliced to in the frontal plane to better visualize the facial prominences during the segmentation step (Figure 4A-D''). Reslicing involves creating a new orthogonal plane at any desired angle through the reconstructed files. It is possible to reduce the number of slices in the stack during reslicing, A new set of files is saved following this step.

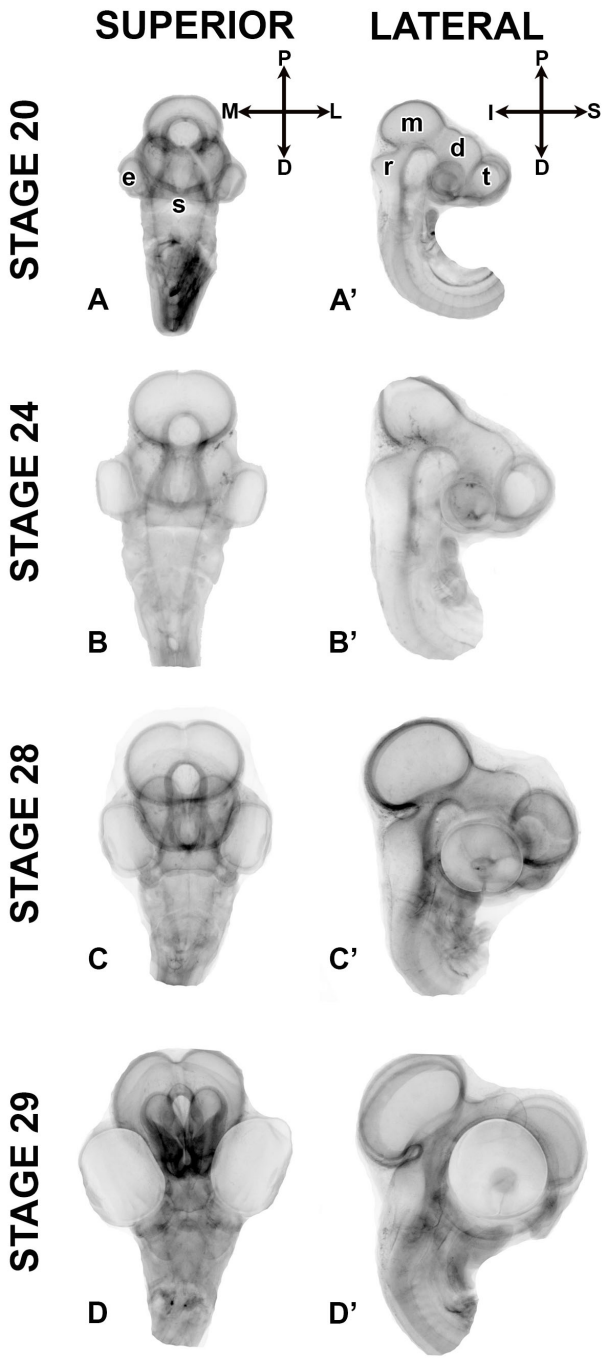

Figure 3 –Projection views from OPT scanner
Whole chick embryos at their respective stages scanned using bright field OPT. Frontal and lateral views shown. d – diencephalon, e – eye, m – mesencephalon, s – stomodeum, r – rhombencephalon, t – telencephalon. Axes: D – distal, I – inferior, L – lateral, M – mesial, P – proximal, S - superior

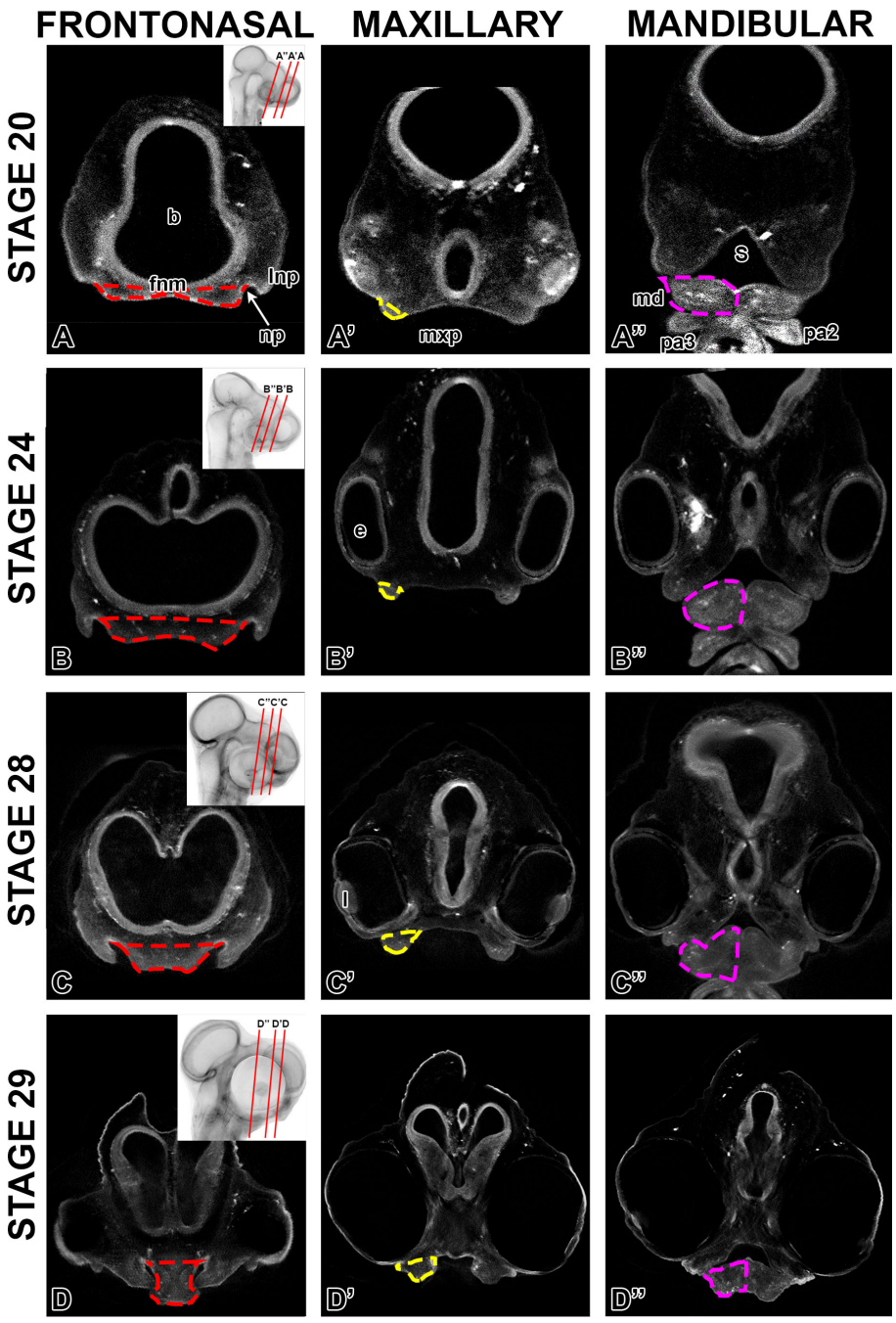

Figure 4 – Slice views, and segmentation of facial prominences
Virtual slices through the head at three levels. Inserts in A, B, C, and D, show lateral views of the corresponding staged chick embryo to reveal the planes of section. The frontonasal mass (red), maxillary (yellow) and mandibular prominences (purple) are outlined with dashed lines. The lines represent areas segmented in Amira. Note that only the right half of the mandibular prominence is outlined, however in Amira the whole mandibular prominence was segmented.

2.4. Segmentation and traditional morphometrics measurements using Amira

Reconstructed and resliced images were imported into Amira (FEI Visualization Sciences Group, Burlington, Maine, USA). Isosurfaces of the full embryo were created from the imported slices (Figure 2). Instead of using a single cutting plane to separate the facial prominences from the rest of the head, individual facial prominences were segmented out. Segmentations were done at multiple planes using a combination of slice and isosurface views to capture the full extent and depth of each prominence. Traditional Morphometrics (TMM) was then conducted to measure the segmented volumes, maximum length and width of the individual facial prominences using functions within Amira. Ratio of length and width was calculated for the frontonasal mass. Segmented facial prominences were then exported to Landmark in the .ply (polygon file format) format.

2.5. Selection of landmarks using Landmark software

Isosurfaces of the individually segmented facial prominences were imported into Landmark 3.6 (Institute for Data Analysis and Visualization, Davis, California, USA). Surface landmarks were chosen based on heights of contour, junctions between facial prominences and grooves (Figure 5; Table 1). The corresponding landmarks could be identified on different stage embryos and thus were considered to be homologous. The landmarks were chosen to best capture the anatomy of the prominences. According to Zedlitch et al. 2012, when landmarking 3D structures, the smallest group size must be less than or equal to 3k-7, where ‘k’ is the number of landmarks in a system or degrees of freedom. Since we need to have at least 5 unique landmarks for each prominence to define its shape, we have 5 degrees of freedom. In three dimensions, there are 3k coordinates. Procrustes superimposition of the 3D data results in the

loss of 7 degrees of freedom which are shared amongst all coordinates (Zelditch et al., 2012). These 7 lost dimensions are differences in size (1), translation in 3 axes (3) and rotation in 3 axes (3). Coordinates of bilaterally homologous landmarks are averaged to avoid inflating the degrees of freedom. Artificially increasing the degrees of freedom which is equivalent to the number of landmarks inflates the significance of the data (Boell et al., 2013; Zelditch et al., 2012). The frontonasal mass and mandibular prominences had 8 landmarks (6 bilaterally symmetric, and 2 midline for a total of 5 unique landmarks), and the lateral nasal and maxillary prominences each had 5 landmarks (5 bilaterally symmetric on the right and left prominences). By keeping the maximum landmarks to 5 we needed to have a sample size of 8 embryos per stage (8 = 3*5 landmarks -7). Landmark files were exported into MorphoJ (Klingenberg, 2011) in the NTSYSpc (numerical taxonomy system for personal computer) format.

2.6. Geometric morphometrics using MorphoJ

The first step in geometric morphometrics was to align the landmarks from each facial prominence across all the stages of embryos to create a Procrustes superimposition for individual facial prominences. We did not create an overall Procrustes superimposition involving all of the facial prominences since we felt this would obscure displacement of landmarks within a particular region of the face. Each facial prominence from a sample embryo was rotated and expanded or contracted to minimize the sum of the squared distances between landmark points. Covariance matrices were created, and Principal component analysis (PCA) carried out. In PCA all the data is included in the analysis and compared to mean centroid size. The centroid of the consensus shape is set to 0,0. The values of the x and y axis are in units of Procrustes distances from the mean/centroid/origin. Using PCA is an unbiased way to see whether there are groups

with distinct shapes amongst the dataset. The mean (consensus shape) is subtracted from each shape to produce "residuals", thereby centering the axes on the mean shape. A covariance matrix of the residuals is then calculated. This estimates the variance and covariance amongst the original variables. Eigenvalues and eigenvectors of the covariance matrix are calculated in order to find the major axes of the data, and the variation among them. PCA rotates the data until 1 new variable (principal component) finds the maximum distance between all the points. The first component is the maximum amount of variance that can be explained by the data. All remaining components are orthogonal to the prior one (ie. 2 is orthogonal to 1 because of 1; 3 is orthogonal to 2 because of 2, because of 1) as a consequence of finding the first principal component. As they are orthogonal, they are considered statistically independent; hence, there is no correlation between the individual components. There are an infinite number of PC axes possible, but each of these explains a diminishing proportion of the variance. Successive principal components contain greater contributions from noise and are thus less informative. The direction and magnitude of change described by each PC can be mapped back to the embryo landmarks to give biological meaning to the variance.

Discriminant function analysis (DFA), and Canonical variate analysis (CVA) maximizes the between-group variance relative to the within group variance. In these analyses, we put in classifiers so that the stage of the embryo was known at the start. These analyses allow the comparison between specific groups of shapes. The number of axes is no longer infinite but is equivalent to the number of groups minus one. In the present study we have 4 stages of embryos minus 1 which leaves us with 3 axes. The advantage of DFA is that an average stage 20 embryo can be created that can be used to compare a reference embryo for another stage. This is particularly important to identify the direction and magnitude of changes in landmarks between

stages. Finally, wireframes are formed around the landmarks to depict the effect of stage on the shape of the individual facial prominences.

2.7. Regression and Statistical analysis

Procrustes ANOVA is a method to quantify the relative amount of variation in the data and to test mean differences (Klingenberg et al., 2002). Implementing a Procrustes ANOVA in MorphoJ results in two interpretations of the ANOVA results: MANOVA statistics, and Goodall's F test statistics.

MANOVA is a multivariate analysis of variance. It attempts to assess the relationship between geometric shape and a categorical predictor variable. Categorical or independent variables are ones that define groups which in the case of this study are the stages of embryos. MANOVA tests for differences in means between multiple groups.

Goodall's F test statistic is based on Procrustes distances, and provides an easy way to quantify the relative magnitude of the effects. F-test is based on the proportion of variance within groups to that between groups. It is of benefit in smaller samples as it has fewer incorporated parameters than MANOVA, but it assumes that variation is similar in all directions at each individual landmark (Klingenberg and Monteiro, 2005). However this assumption in shape change is unrealistic for biological models, as individual landmarks behave independently of one another (Klingenberg and Monteiro, 2005). Instead, Goodall's F test is nevertheless useful to measure the relative magnitude of effects, while MANOVA is used to make statistical inferences.

Regression is often used to correct for the effects of size on shape. Size correction in GMM usually uses a regression of shape on centroid size, and sometimes on log-transformed

centroid size. The choice is dependent on which one produces the better linear relationship. Since we are using embryos of varying size ranges, shape change may be disproportionately distributed within our stages. To test the influence of size on shape, a multivariate linear regression of the Procrustes shape coordinates on log determined centroid size was performed.

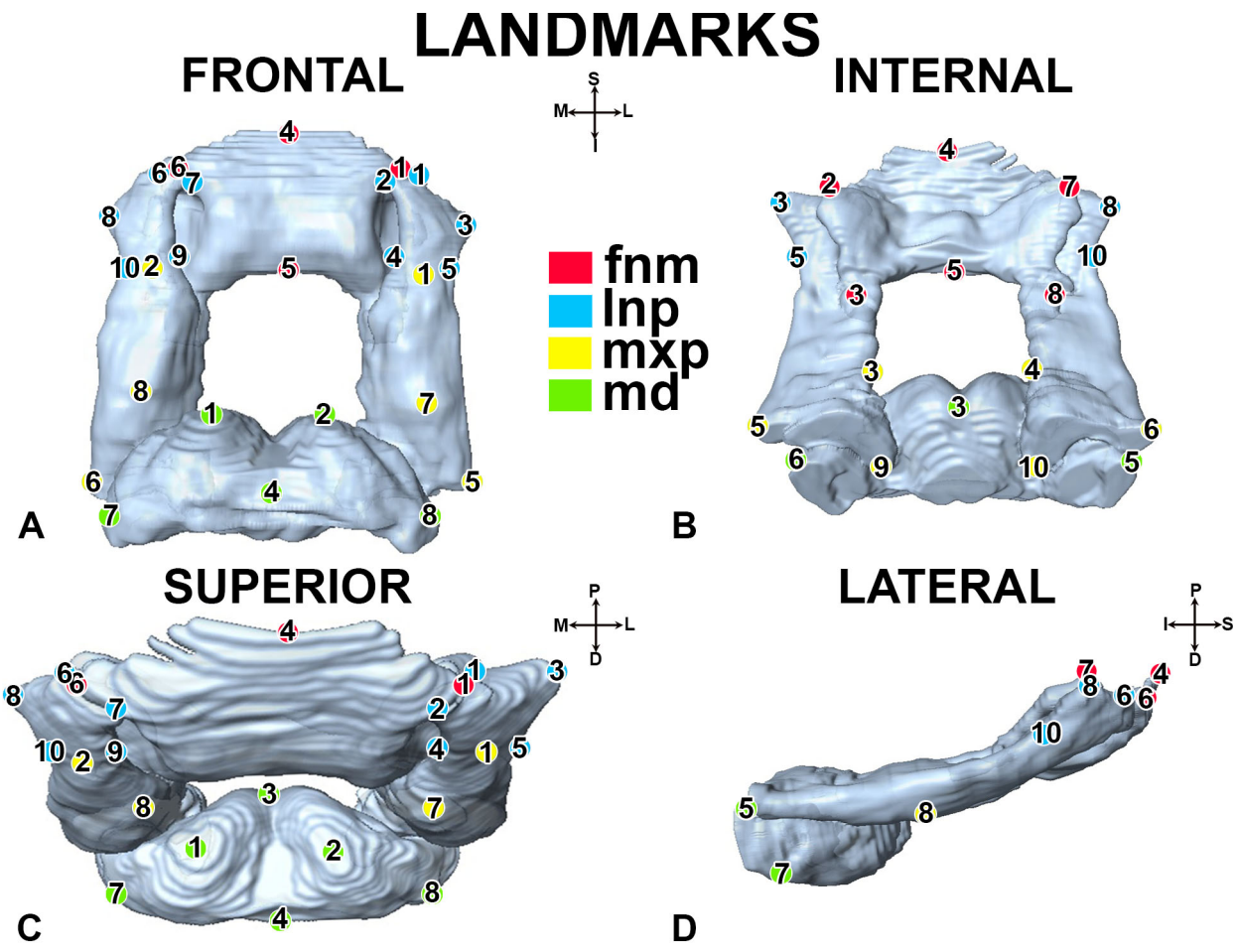

Figure 5 – Individual landmarks numbered on individual facial prominences. Frontonasal mass landmarks in red, lateral nasal prominence landmarks in blue, maxillary prominence landmarks in yellow, and mandibular prominence landmarks in green. Refer to Table 1 for locations of individual landmarks on each facial prominence. Axes: D – distal, I – inferior, L – lateral, M – mesial, P – proximal, S - superior

A. FRONTONASAL MASS – 5 paired and 2 unique landmarks		
Landmark 1:	paired with landmark 6	Left lateral-most junction between FNM and LNP
Landmark 2:	paired with landmark 7	Left inferior-most junction between FNM and LNP
Landmark 3:	paired with landmark 8	Left inferior maximum curvature nasal pit
Landmark 4:	unpaired	Superior midline
Landmark 5:	unpaired	Inferior midline
Landmark 6:	paired with landmark 1	Right lateral-most junction between FNM and LNP
Landmark 7:	paired with landmark 2	Right inferior-most junction between FNM and LNP
Landmark 8:	paired with landmark 3	Right inferior maximum curvature nasal pit
B. LATERAL NASAL PROMINENCE - 10 paired landmarks		
Landmark 1:	paired with landmark 6	Left superior-lateral maximum curvature
Landmark 2:	paired with landmark 7	Left superior-medial junction between LNP&FNM
Landmark 3:	paired with landmark 8	Left lateral maximum curvature
Landmark 4:	paired with landmark 9	Left inferior maximum curvature
Landmark 5:	paired with landmark 10	Left inferior-medial junction between LNP and MXP
Landmark 6:	paired with landmark 1	Right superior-lateral maximum curvature
Landmark 7:	paired with landmark 2	Right superior-medial junction between LNP and FNM
Landmark 8:	paired with landmark 3	Right lateral maximum curvature
Landmark 9:	paired with landmark 4	Right inferior maximum curvature
Landmark 10:	paired with landmark 5	Right inferior-medial junction between LNP and MXP
C. MAXILLARY PROMINENCE - 10 paired landmarks		
Landmark 1:	paired with landmark 2	Left junction between LNP and MXP
Landmark 2:	paired with landmark 1	Right junction between LNP and MXP
Landmark 3:	paired with landmark 4	Left medial maximum curvature
Landmark 4:	paired with landmark 3	Right medial maximum curvature
Landmark 5:	paired with landmark 6	Left dorsal-lateral maximum curvature
Landmark 6:	paired with landmark 5	Right dorsal-lateral maximum curvature
Landmark 7:	paired with landmark 8	Left inferior maximum curvature
Landmark 8:	paired with landmark 7	Right inferior maximum curvature
Landmark 9:	paired with landmark 10	Left medial junction with MD
Landmark 10:	paired with landmark 9	Right medial junction with MD
D. MANDIBULAR PROMINENCE – 6 paired and 2 unique landmarks		
Landmark 1:	paired with landmark 2	Right center maximum curvature
Landmark 2:	paired with landmark 1	Left center maximum curvature
Landmark 3:	unpaired	Superior midline
Landmark 4:	unpaired	Inferior midline
Landmark 5:	paired with landmark 6	Right superior-lateral junction with MXP
Landmark 6:	paired with landmark 5	Left superior-lateral junction with MXP
Landmark 7:	paired with landmark 8	Right inferior-lateral maximum curvature
Landmark 8:	paired with landmark 7	Left inferior-lateral maximum curvature

Table 1 – Landmarks for all specimens
Location of landmarks on individual prominences for all stages of embryos. FNM – frontonasal mass, LNP – lateral nasal prominence, MXP – maxillary prominence, MD – mandibular prominence. The frontonasal mass (1.A) and mandibular prominence (1.D) have 8 landmarks. 6 were bilaterally symmetric, and 2 were along the midline of the prominence. The lateral nasal prominence (1.C) and maxillary prominence (1.D) have 10 landmarks. All 10 were bilaterally symmetric and therefore represent 5 unique landmarks.

Chapter 3: Results

3.1 Experimental Rationale: Choice of stages, sample size

Our starting point for the study was stage 20, as this is near the beginning of facial prominence morphogenesis in the chick embryo, and a time where minimal connective tissue differentiation has occurred. This was also a time where the contours of the individual facial prominences could be readily differentiated and nasal pits are just starting to invaginate (Figure 2A-A''). The maxillary process is distinct, and equals or exceeds the mandibular process in length. By stage 24, the facial prominences have enlarged and there are distinct grooves between the lateral nasal and maxillary prominence (Figure 1B-B''). There is a prominence midline groove in the mandibular prominence and the frontonasal mass is flat with the corners in contact but not yet fused with adjacent prominences. By stage 28, the shape of the beak is more pronounced as globular processes/protrusions from the corners of the frontonasal mass are now contacting the maxillary prominences. The mandibular prominences have also lengthened and grown forward (Figure 1C-C''). At stage 29, the upper beak is narrower, is more prominent, and is in contact with the mandibular prominence. The mandibular prominences have also lengthened, and fused with the second pharyngeal arch (Figure 1D-D''). The chick face narrows considerably between stages 20-29 bringing the eyes closer to the midline. After stage 29, the upper and lower beaks begin to form cartilage and project out from the head. The shape is therefore dramatically different. Another reason for selecting stages 20-28 is that these early stages are when beak patterning is taking place whereas at stage 29 and afterwards, it is just growth of the skeleton that is driving beak enlargement. The most likely stages when cellular rearrangements are taking place are between stage 20 and 28 based on data from McGonnell

(McGonnell et al., 1998). By adding one additional stage we include lip fusion which is also a significant event.

3.2 Power Analysis

Based on preliminary data from maxillary prominence segmentations (Geetha-Loganathan et al., 2014), the minimum sample size to demonstrate significant statistical difference in linear measurements or volumes between stage 24 and 28 maxillary prominences was 2. The reason the number of embryos needed is so low is that there are very large differences in absolute size of the embryo between these stages. This can be easily seen by observing the embryo in the egg.

In this study we did not limit the analysis to traditional linear or volumetric measurements, but instead wanted to measure shape change. In order to accomplish this we needed to calculate sample size differently. We determined that 5 landmarks was the minimum needed to define the morphology of a facial prominence. Therefore based on the Zelditch formula (N = (3*number of landmarks)-7) our sample size was a minimum of 8 embryos per each of the 4 stages for a total of 32 chick embryos.

3.3 Traditional Morphometrics

Traditional morphometrics were conducted using segmented facial prominences created in Amira. Volumetric analysis, and 2D linear ratios were conducted on the segmented facial prominences (Table 2A, 2B). The frontonasal mass had a 635% increase in volume from stage 20 to 29, the lateral nasal prominence had a 2486% increase in volume from stage 20 to 29, the maxillary prominence had a 1379% increase in volume from stage 20 to 29, and the mandibular prominence had a 1356% increase in volume from stage 20 to 29. The greatest volumetric

change amongst facial prominences was within the lateral nasal prominences, and the smallest volumetric change was within the frontonasal mass.

When looking at 2D linear data of the frontonasal mass, there is an increase in medio-lateral width from stage 20 to stage 28, then a sharp decrease at stage 29. The superior-inferior height of the frontonasal mass increases from stage 20 to stage 29. Stated another way, the ratio of ml/si length increased 3.5-fold between stages 20 and 29 (Table 2B).

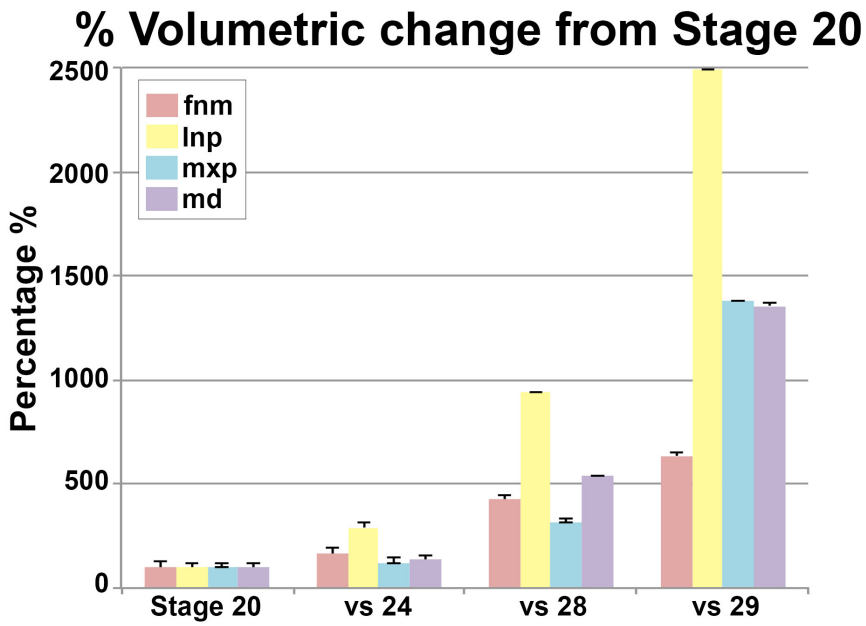

Figure 6 – Percentage volumetric change
Percentage volumetric change of individual facial prominences compared against their respective stage 20 facial prominences. Red – frontonasal mass, yellow – lateral nasal prominence, blue – maxillary prominence, purple – mandibular prominence. Each individual facial prominence enlarges as the embryo grows from stage 20 to stage 29. The lateral nasal prominence has the greatest percentage increase in volume. There is rapid volumetric enlargement occurring between stage 28 and stage 29 for all facial prominences.

Volumetric measurements						
A	**Stage 20 (mm^3)**	**Stage 24 (mm^3)**	**Stage 28 (mm^3)**	**Stage 29 (mm^3)**	**% change 20-28**	**% change 20-29**
FRONTONASAL MASS	0.091±0.023	0.149±0.039	0.386±0.076	0.578±0.090	**424%**	**635%**
LATERAL NASAL PROMINENCE	0.022±0.005	0.064±0.014	0.207±0.002	0.547±0.038	**941%**	**2486%**
MAXILLARY PROMINENCE	0.091±0.018	0.107±0.028	0.285±0.054	1.255±0.054	**313%**	**1379%**
MANDIBULAR PROMINENCE	0.123±0.020	0.164±0.038	0.660±0.005	1.668±0.160	**537%**	**1356%**

B	**Stage 20 (mm)**	**Stage 24 (mm)**	**Stage 28 (mm)**	**Stage 29 (mm)**
Average medio-lateral length (mm)	1.66	1.99	2.36	1.29
Average superior-inferior length (mm)	0.66	0.97	1.42	1.83
ratio ml/si length	2.51	2.06	1.67	0.71
% Change of Ratio				
Stage 20		122	150	354
Stage 24			123	290
Stage 28				235

Table 2 - Traditional Morphometrics

A – Volumetric Changes of the facial prominences amongst Stage 20, 24, 28, and 29 embryos. Table of TMM completed in Amira showing volumetric differences amongst stages and prominence. The greatest change in volume from is seen in the lateral nasal prominence as it transitions from stage 20 to 28, and 20-29.

B – Linear dimensional changes of the frontonasal mass. Average length in the medio-lateral and superior-inferior axes was measured at stages 20, 24, 28, and 29 in the frontonasal mass. There is a 3.5 fold change in the ml/si ratio as the frontonasal mass transitions from stage 20 to 29.

3.4 Quality Control of landmarking

Intra-observer reliability was assessed with a single operator. In order to assess the repeatability of the landmarks, we performed eight repeated trials of a randomly selected stage 20, and 24 embryo, and three repeated trials of three randomly selected stage 20 and stage 24 embryos. We concentrated on the maxillary prominence of stage 20 and stage 24 embryos, as the shape of the maxillary prominence had the least number of distinct features and the selection of homologous landmarks was most challenging.

Since we used Procrustes superimposed landmarks in the analysis, we quantified measurement error as the variation in landmark position as a proportion of the total variation in our sample. Measurement error is artificially minimized when comparing between very dissimilar stages; hence, we compared embryos of very similar stages.

PCA analysis of the stage 20 maxillary prominence showed that most of the variation in landmarking is along the mediolateral axis, whereas for the stage 24 maxillary prominence, most of the variation is uniform (Fig. 7A). The 95% confidence ellipses for each stage reveal that the shape of stage 20 and stage 24 maxillary prominences are quite similar to one another. Importantly, the differences between repeated trials are very small, compared to the differences among individuals (Fig.7B). Due to the arbitrary nature of the X and Y units for PCA it is necessary to integrate the repeated measures data into the PCA of the maxillary prominence for all stages (Fig. 7C). In this way the scale of the two datasets is equivalent. This analysis showed that the randomly repeated measurements fall within the respective 95% confidence ellipse for their representative stage and are tightly clustered. The shape variation we detected between stages was therefore mainly due to differences in shape, and not due to variation in the placement of landmarks.

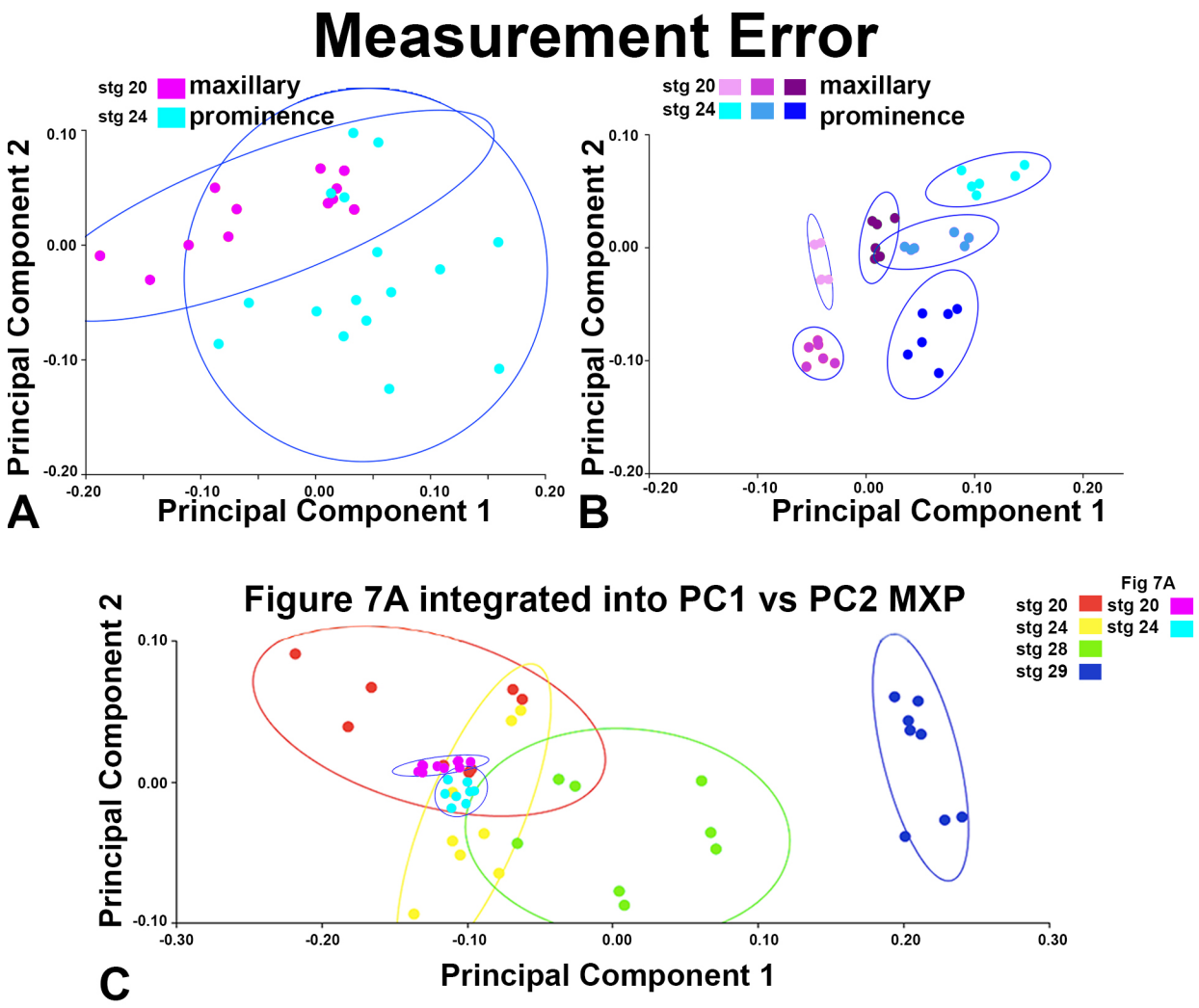

Figure 7 – Measurement error

A – PCA of a randomly selected stage 20 and stage 24 maxillary prominences repeated eight times. All 16 points (8 right and 8 left) for each maxillary prominence fall within their respective 95% confidence ellipse.

B – PCA of three randomly selected stage 20 and stage 24 maxillary prominences repeated three times, revealing that differences in repeated trials are small, compared to differences among individuals.

C – PCA of Figure 7A (randomly selected stage 20 and 24 embryos repeated 8 times) superimposed and integrated into PCA of maxillary prominence for all stages, revealing that they still fall within the respective 95% confidence ellipse for their respective stages, and are tightly clustered. There are now 8 points for each randomly selected stage 20 and 24 maxillary prominence, as we are comparing the combined right and left side against the other maxillary prominences from the other stages. Point 0,0 is now shifted towards an older stage, as there is greater weighting from the stage 28 and stage 29 maxillary prominences in the PCA analysis. .

3.5 Procrustes Superimposition

Procrustes Superimposition (PS) minimizes the shape differences amongst a sample due to orientation and scale but not allometry. PS must be conducted prior to PCA, CVA, and DFA as it identifies the consensus/centroid shape of the sample. Once PS is done, we will need to perform a regression against centroid size, which essentially removes allometry and highlights differences in shape between stages. The lowest number for Procrustes sum of squares (PSS) is 0, which would indicate that objects within a dataset have identical shapes. A larger PSS would indicate a greater difference in shape amongst objects within a group as seen for the frontonasal mass and mandible at stage 29 (Fig. 8A,9B). The PSS is similar to a least-squares fit of a regression line. A larger PSS indicates greater shape variation within objects of a dataset. Expressed in quantitative terms, the PSS of the frontonasal mass is 1.63 (Table 3), the lateral nasal prominence PSS is 0.23 (Table 4), the maxillary prominence PSS is 0.89 (Table 4), and the mandibular prominence PSS is 1.30 (Table 3). Hence, the frontonasal mass and the mandibular prominences have a greater shape differences between the 4 stages of development than do the lateral nasal and maxillary prominences (Fig. 8, 9).

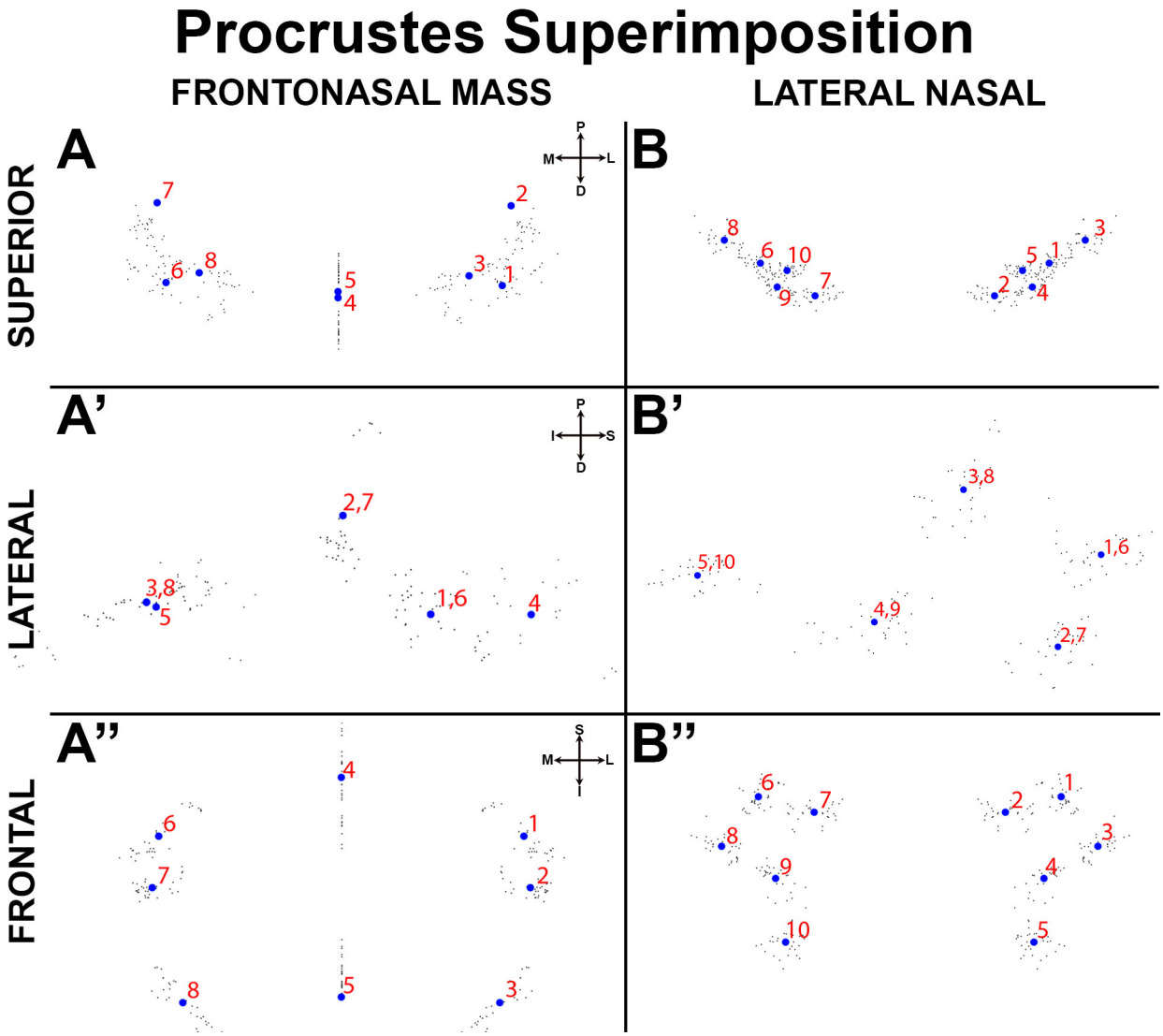

Figure 8 – Procrustes Superimposition
Procrustes Superimposition of the frontonasal mass and lateral nasal prominences for stages 20, 24, 28, and 29. MorphoJ uses a full Procrustes fit aligned by principal axes, and projects the data to the tangent space by orthogonal projection. It is generally a consensus of landmarks, with corresponding data clouds shown for each individual landmark. Procrustes Superimposition minimizes the shape difference (Procrustes distance) between objects. The blue dots represent the mean landmark positions, and the small black points/cloud, represent the landmark positions for individual specimens in the sample. Frontonasal mass (A,A',A'') and lateral nasal prominence (B,B', B'') are shown in the superior, lateral, and frontal plane. Axes: D – distal, I – inferior, L – lateral, M – mesial, P – proximal, S - superior

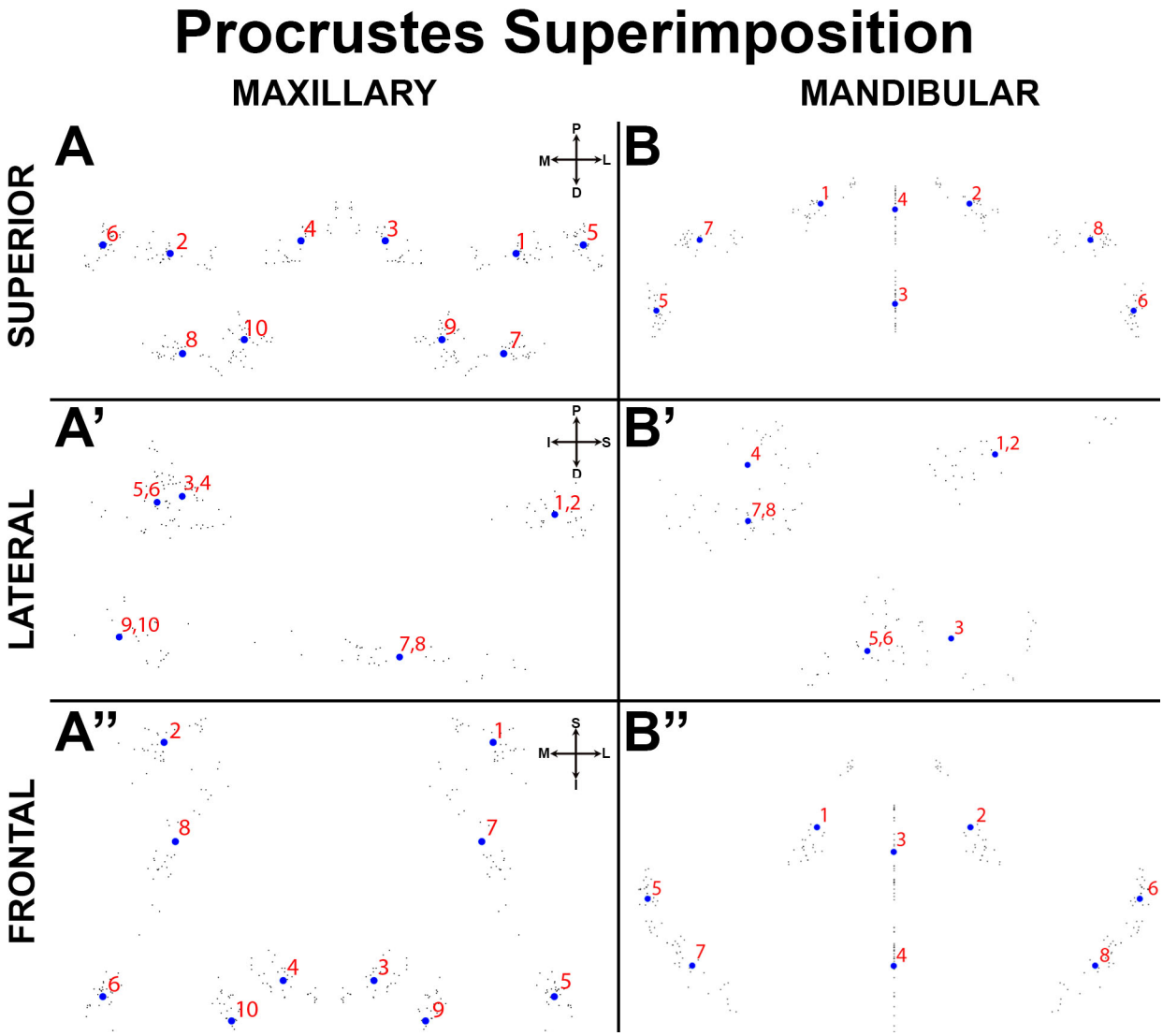

Figure 9 – Procrustes Superimposition
Procrustes Superimposition of the maxillary prominence and mandibular prominences for Stages 20, 24, 28, and 29. MorphoJ uses a full Procrustes fit aligned by principal axes, and projects the data to the tangent space by orthogonal projection. It is generally a consensus of landmarks, with corresponding data clouds shown for each individual landmark. Procrustes Superimposition minimizes the shape difference (Procrustes distance) between objects. The blue dots represent the mean landmark positions, and the small black points/cloud, represent the landmark positions for individual specimens in the sample. Maxillary prominence (A,A',A'') and mandibular prominence (B,B', B'') are shown in the superior, lateral, and frontal plane. Axes: D – distal, I – inferior, L – lateral, M – mesial, P – proximal, S - superior

	Frontonasal Mass			*Mandibular Prominence*		
Landmark	**Axis 1 (x)**	**Axis 2 (y)**	**Axis 3 (z)**	**Axis 1 (x)**	**Axis 2 (y)**	**Axis 3 (z)**
1	0.37	0.14	-0.03	-0.15	0.14	0.10
2	0.38	0.03	0.08	0.15	0.14	0.10
3	0.32	-0.20	-0.02	0.00	0.10	-0.10
4	0.00	0.25	-0.03	0.00	-0.13	0.09
5	0.00	-0.19	-0.03	-0.49	0.00	-0.12
6	-0.37	0.14	-0.03	0.49	0.00	-0.12
7	-0.38	0.03	0.08	-0.40	-0.13	0.03
8	-0.32	-0.20	-0.02	0.40	-0.13	0.03
	PSS = **1.63**			PSS = **1.30**		

Table 3 – Procrustes Superimposition for the frontonasal mass and mandibular prominence
Cartesian coordinates (x,y,z) of the landmarks on the mean shape across all stages. Procrustes sum of squares (PSS) indicates the variation in shape amongst stages 20, 24, 28, and 29. The frontonasal mass and mandibular prominence have 8 landmarks as there are 3 pairs of bilaterally symmetric landmarks, and 2 unique midline landmarks. Refer to Table 1.

	Lateral Nasal Prominence			*Maxillary Prominence*		
Landmark	**Axis 1 (x)**	**Axis 2 (y)**	**Axis 3 (z)**	**Axis 1 (x)**	**Axis 2 (y)**	**Axis 3 (z)**
1	0.32	0.08	0.01	0.29	0.26	0.04
2	0.25	0.06	-0.03	-0.29	0.26	0.04
3	0.37	0.01	0.04	0.12	-0.09	0.06
4	0.30	-0.03	-0.02	-0.12	-0.09	0.06
5	0.28	-0.12	0.00	0.38	-0.12	0.06
6	-0.32	0.08	0.01	-0.38	-0.12	0.06
7	-0.25	0.06	-0.03	0.27	0.11	-0.09
8	-0.37	0.01	0.04	-0.27	0.11	-0.09
9	-0.30	-0.03	-0.02	0.19	-0.15	-0.07
10	-0.28	-0.12	0.00	-0.19	-0.15	-0.07
	PSS =**0.23**			PSS =**0.89**		

Table 4 – Procrustes Superimposition for the lateral nasal and maxillary prominences.
Cartesian coordinates (x,y,z) of the landmarks on the mean shape across all stages. Procrustes sum of squares indicates the variation in shape amongst stages 20, 24, 28, and 29. The lateral nasal prominence and maxillary prominence have 10 landmarks, as there are 5 pairs of bilaterally symmetric landmarks. Refer to Table 1.

3.6 Principal Component Analysis

We have chosen to display the results of PCA in three formats: Principal component 1 (PC1) vs Principal component 2 (PC2) scatterplot, wireframe, and text output. PC1 and PC2 capture 70-90% of the variation in the data as shown by the eigenvalues (Table. 5A-D). In scatterplots the general trend was that the different stages of embryos grouped with each other. This is an unbiased assessment of shape differences in the entire sample i.e. we did not inform the software of the identity of the embryos. In looking at individual facial prominences there are some interesting trends. For the frontonasal mass, maxillary prominence, and mandibular prominences (Figure 10A,C,D), the shapes of the stage 20, 24, and 28 facial prominences segregate clearly from those of stage 29 embryos. For the lateral nasal prominence (Figure 10B), the shapes of the stage 20, 24, 28, and 29 are similar as the ellipses overlap. Interestingly, there is minimal shape difference between stages 24 and 28, therefore the prominence appears to enlarge fairly evenly between these two stages (isometric or even displacement of the landmarks in all three dimensions).

The illustration of where the shape changes are occurring relative to landmarks is shown in wire frame drawings (Figure 11). Here, the PC1 of each prominence is arbitrarily set to 0.1 Procrustes distance away in a positive direction (dark blue) from the mean (light blue) . When we relate wireframe back to the scatter plot in figure 10, we notice that for the frontonasal mass, lateral nasal and mandibular prominences, the stage 29 data points are negative to the stage 20-28 data points. Therefore the mean wireframe for these facial prominences is closer to a stage 20-28. In the case of the maxillary prominence the stage 29 data is positive relative to the other stages. Therefore the wireframe shows that the average shape is transitioning away from stages

20-28 towards a stage 29 shape. All facial prominences undergo a significant change in shape from the mean as shown by Goodall's F test and MANOVA calculations (Table 6). Note that we only calculated variability in PC1 and variations on one principal component are statistically uncorrelated with variation on another principal component. However since PC1 covers the largest degree of variation, it is unnecessary to make such statistical calculations for the other PCs.

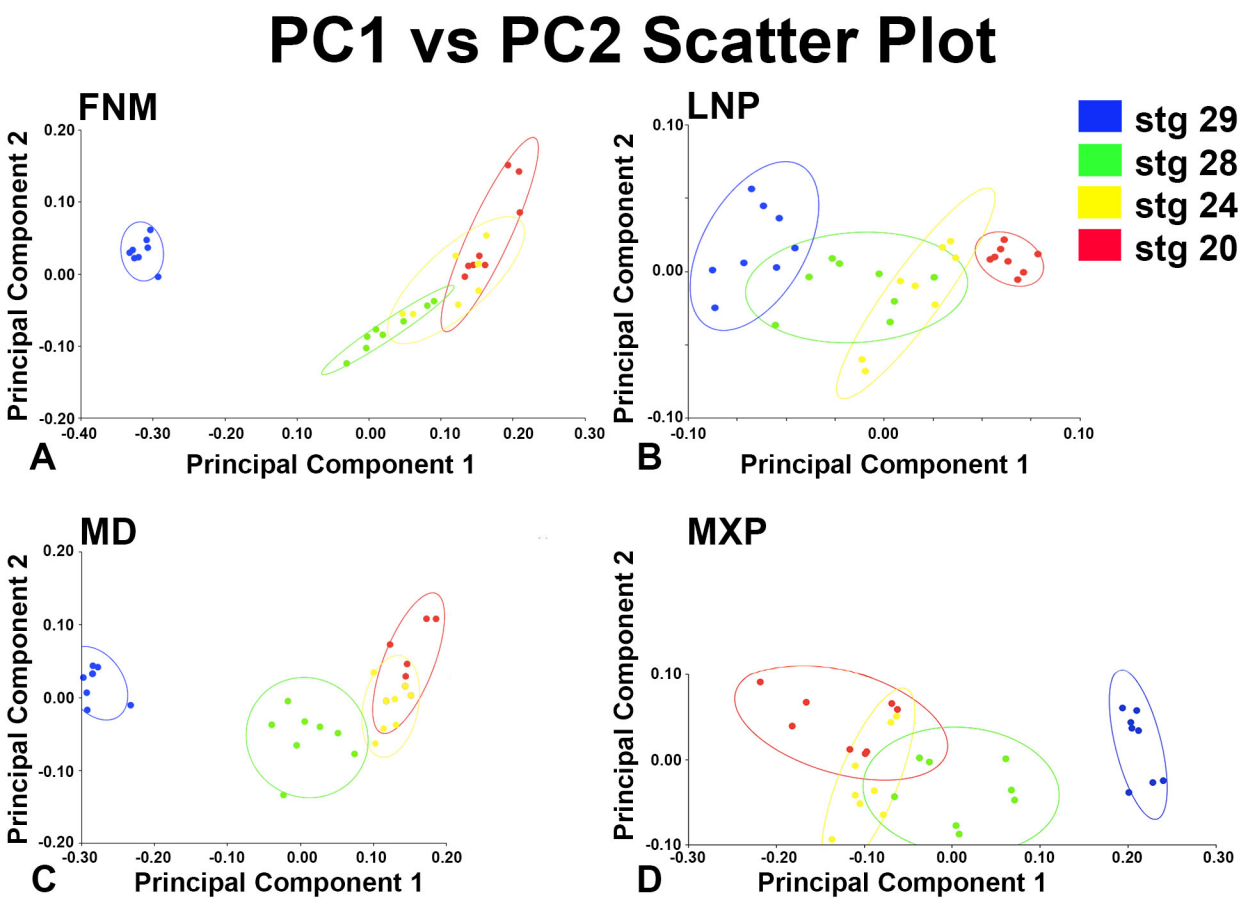

Figure 10 – PCA – PC1 vs PC2
Graphical scatter plot output of the Principal Component Analysis of each of the individual facial prominences. PC1 is compared against PC2 as it contains the greatest amount of variability in the data set, and is most useful in identifying relationships between samples. The major differences are seen between stage 29 and 28 in the frontonasal mass and mandibular prominences. This suggests that these two parts of the face explain the majority of appearance changes occurring at stage 29. Stage 20 – red, Stage 24 – yellow, Stage 28 – green, Stage 29 – blue. The centroid of the consensus shape is at 0,0. A – PC1 vs PC2 of frontonasal mass. B – PC1 vs PC2 of lateral nasal prominence. C – PC1 vs PC2 of the mandibular prominence. D – PC1 vs PC2 of the maxillary prominence.

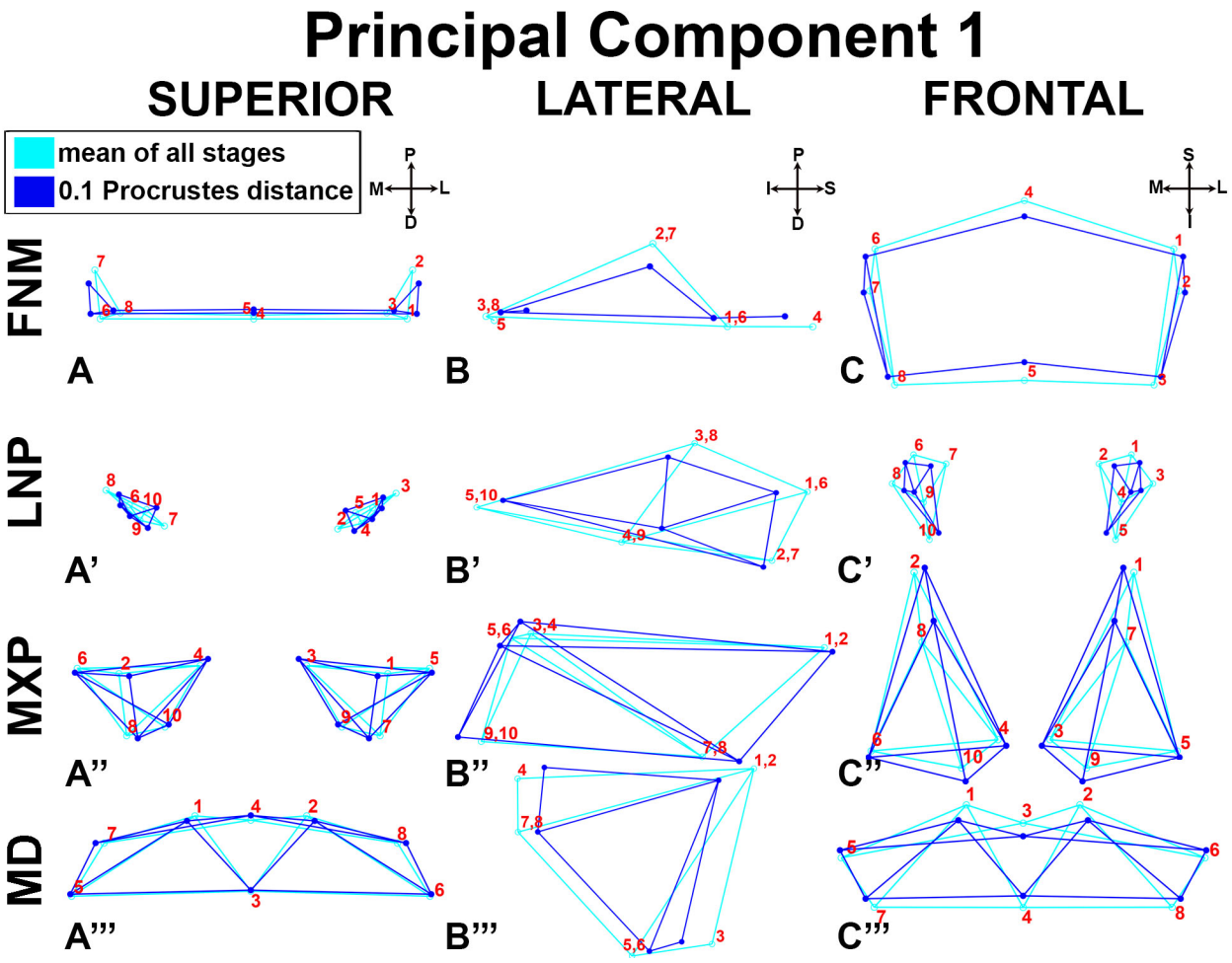

Figure 11 – PCA –Wireframe graph of PC1
PC1 of the individual facial prominences along the superior, lateral, and frontal plane. Light blue is the mean/consensus shape from stages 20,24,28 and 29. The navy blue is +0.1 Procrustes distance away from the mean. 0.1 Procrustes distance corresponds to a change of principal component score by 0.1 units in the positive direction. The blue dots and the red numbers indicate the landmarks chosen for each individual facial prominence. Landmarks are only placed on the mean shape, and their change in location is interpolated onto the navy blue wireframe shape. Axes: D – distal, I – inferior, L – lateral, M – mesial, P – proximal, S - superior

A. PCA – Frontonasal Mass			
Principal Component	**Eigenvalues**	**% Variance**	**Cumulative %**
1	0.03798	**81.5**	81.5
2	0.00415	**8.9**	90.4
3	0.00168	**3.6**	94.0
4	0.00105	**2.3**	96.3
5	0.00068	**1.5**	97.8
6	0.00051	**1.1**	98.9
7	0.00032	**0.7**	99.6
8	0.00014	**0.4**	100.0
Total Variance	**0.04660**		
B. PCA – Lateral Nasal Prominence			
Principal Component	**Eigenvalues**	**% Variance**	**Cumulative %**
1	0.00376	**59.1**	59.1
2	0.00069	**10.8**	69.8
3	0.00057	**9.0**	78.8
4	0.00052	**8.2**	87.0
5	0.00032	**5.0**	92.0
6	0.00020	**3.2**	95.3
7	0.00012	**1.8**	97.1
8	0.00009	**1.4**	98.5
9	0.00006	**0.9**	99.4
10	0.00003	**0.4**	99.8
11	0.00001	**0.2**	100.0
Total Variance	**0.00637**		
C. PCA – Maxillary Prominence			
Principal Component	**Eigenvalues**	**% Variance**	**Cumulative %**
1	0.01956	**77.0**	76.971
2	0.00253	**10.0**	86.937
3	0.00089	**3.5**	90.426
4	0.00082	**3.3**	93.68
5	0.00051	**2.0**	95.681
6	0.00038	**1.5**	97.166
7	0.00027	**1.1**	98.24
8	0.00018	**0.7**	98.962
9	0.00014	**0.5**	99.494
10	0.00008	**0.3**	99.793
11	0.00005	**0.2**	100
Total Variance	**0.02541**		

D. PCA – Mandibular Prominence			
Principal Component	**Eigenvalues**	**% Variance**	**Cumulative %**
1	0.03064	**81.1**	81.1
2	0.00266	**7.0**	88.2
3	0.00153	**4.0**	92.2
4	0.00115	**3.0**	95.3
5	0.00076	**2.0**	97.3
6	0.00058	**1.5**	98.8
7	0.00020	**0.5**	99.4
8	0.00013	**0.3**	99.7
9	0.00011	**0.3**	100.0
Total Variance	**0.03776**		

Table 5 – Principal Component Analysis
Principal Component Analysis (PCA) showing the number of principal components, the corresponding eigenvalues, the amount of variance in % it accounts for, and the cumulative % of total variance. The table shows varying number of PCs for each facial prominence as MorphoJ rounds off the number of PCs to account for 100% cumulative variation.
A - PCA of the frontonasal mass reveals 8 principal components that account for 100% of the variance in shape. Principal component 1 (PC1) alone accounts for 81.5% of the shape variation amongst the frontonasal mass. Principal component 2 (PC2) accounts for 8.9% of the shape variation. PC1 and PC2 account for 90% of the variance of the frontonasal mass.
B - PCA of the lateral nasal prominence reveals 11 principal components that account for 100% of the variance in shape. PC1 accounts for 59.1% of the shape variation. PC2 accounts for 10.8% of the shape variation. PC1 and PC2 account for 70% of the variance of the lateral nasal prominence.
C - PCA of the maxillary prominence reveals 11 principal components that account for 100% of the variance in shape. PC1 accounts for 77.0% of the shape variation. PC2 accounts for 10.0% of the shape variation. PC1 and PC2 account for 87% of the variance of the maxillary prominence.
D - PCA of the mandibular prominence reveals 9 principal components that account for 100% of the variance in shape. PC1 accounts for 81.1% of the shape variation. PC2 accounts for 7.0% of the shape variation. PC1 and PC2 account for 88.2% of the variance of the mandibular prominences.

3.7 Regression Analysis

GMM removes scale, but there is still shape heterogeneity in our samples due to size differences. This allometric component can be removed using the residuals of a multivariate regression on the covariate; centroid size, for statistical comparisons. Regressions of shape on centroid size showed that we could still distinguish shapes of the facial prominences by stage as shown by the clustering of the majority of specimens with others of their own stage (Fig. 12A-D). Several differences were noted compared to the PCA analysis. The stages each cluster together except for stage 20 embryos which were more spread out. There some outliers in the stage 20 sample that may be older than the others and therefore overlap with the stage 24 samples. Thus some of the shape variability in stage 20 embryos could be attributed to size. The stage 29 frontonasal mass, maxillary and mandibular prominences are distinct from the other stages (Fig. 12 A,C,D) as was shown in the PCA analysis (Fig. 10).

In addition embryos were observed to fall along a well-defined exponential growth curve for the frontonasal mass, and maxillary and mandibular prominences. The lateral nasal prominence was the only prominence in which the data did not describe a curve. This fits with our finding that shape differences in the lateral nasal prominence were rather minor.

Principal component analysis of the size residuals demonstrated differentiation along principal component 1 (PC1), supporting our original PCA. Therefore it is possible to predict the stage of an embryo just by determining the shape of either the frontonasal mass, maxillary or mandibular prominences but not the lateral nasal prominence. Such a reverse analysis will be very useful in future studies where embryos are collected a certain number of hours post manipulation and not necessarily according to stage.

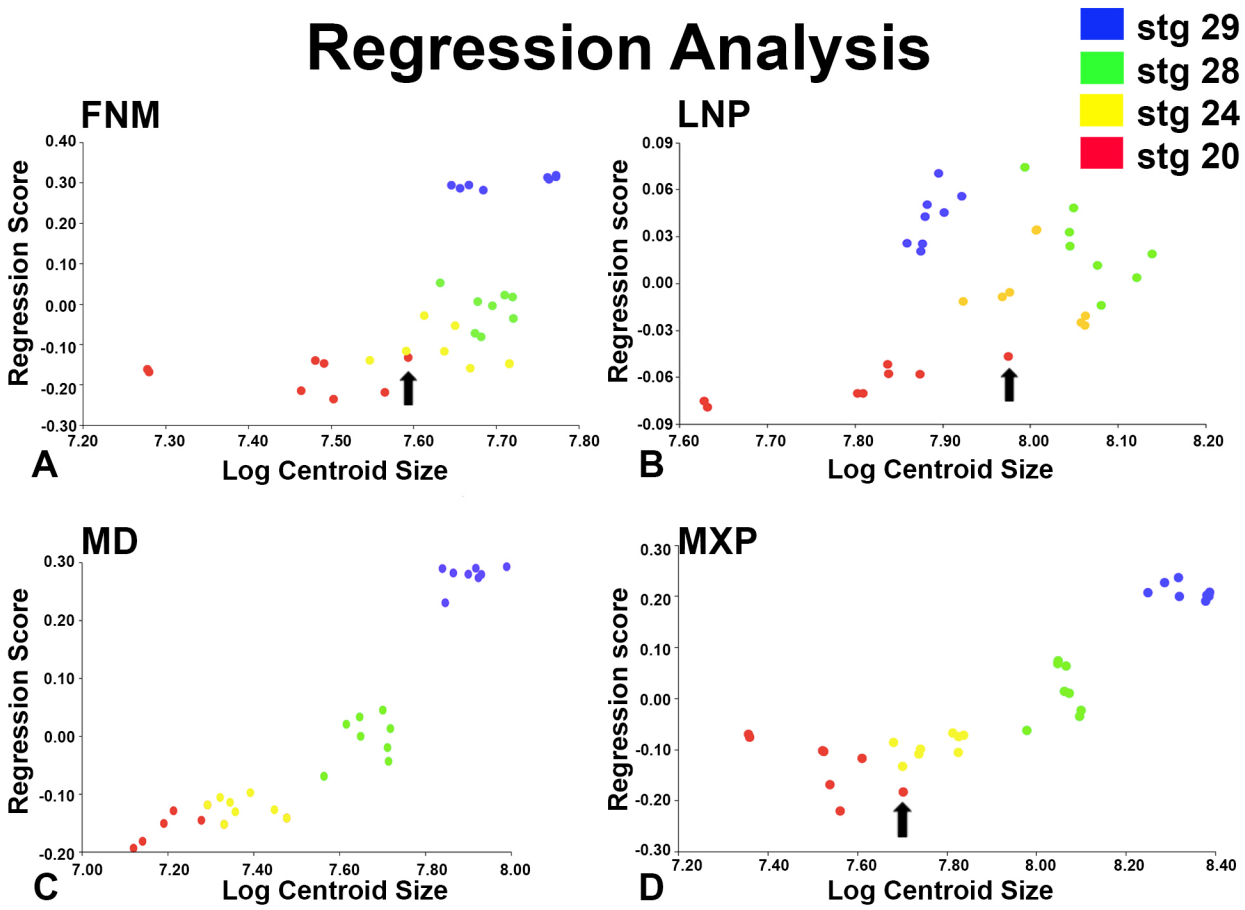

Figure 12 – Regression Analysis
Regressions of shape on log-determined centroid size estimate allometry within each of the facial prominences. The positive slope of the regressions for each of the facial prominences demonstrates that shape change scales with size. The stages cluster together, except for the stage 20 embryos that are more spread out. In A and D the stage 20 embryo indicated by the black arrow is the same so this specimen may be an outlier relative to other stage 20 embryos (for example, a stage 22). In B this is a different stage 20 embryo than in A and D. This second stage 20 embryo (arrow in B) is less likely to be a true outlier since it only appears out of the main group in the lateral nasal prominence shape analysis.

	Procrustes ANOVA		*MANOVA*
	Goodall's F test	P(param.)	P(param.)
Frontonasal Mass	194.14	<0.0001	<0.0001
Lateral nasal prominence	21.69	<0.0001	<0.0001
Maxillary prominence	104.49	<0.0001	<0.0001
Mandibular prominence	304.04	<0.0001	<0.0001

Table 6 – Goodall's F test and MANOVA
Goodall's F test and MANOVA to ascertain significance of variance of shape on individual facial prominences across stages 20, 24, 28, and 29. Goodall's F test reveals the magnitude of the shape differences, and MANOVA is used for statistical inference

3.8 Canonical Variate Analysis

We have chosen to display the results of the CVA in three formats: Canonical variate 1 (CV1) vs Canonical variate 2 (CV2) scatterplot, wireframe, and text output. CV1 captures 80-93% of the variation in the data as shown by the eigenvalues (Table. 7A-D). In CVA, groups are defined a priori. The general trend in the scatterplots was that different stages of embryos grouped with each other. This is another unbiased assessment of shape differences in the entire sample, whereby groups are defined a priori unlike in PCA. In looking at the individual facial prominences, there are some interesting trends. For the frontonasal mass, maxillary prominence, and mandibular prominence (Figure 12A,C,D), the shapes of the stage 20, 24, and 28 facial prominences are segregated clearly from the stage 29 embryos just like in the PCA scatterplot (Figure 10A,C,D). For the lateral nasal prominence (Figure 12B), the shape of the stage 20 is distinct from the stage 24, 28, and 29 prominence. This is different from the PCA of the lateral nasal prominence (Figure 10B), where all the stages are similar, and the group is not defined prior to the analysis. Interestingly, there is no shape difference between stage 20 and 24 of the frontonasal mass, maxillary prominence, and mandibular prominence, but there is shape difference in the lateral nasal prominence. This is different from the PCA, as there were minimal shape differences between stage 20 and 24 for all the facial prominences.

In figure 13, a wireframe graph shows the shape changes occurring relative to the landmarks as it progresses positive 10 Mahalanobis units (dark blue) away from the mean shape (light blue). It is important to refer back to the CVA graphs to interpret the wireframes since the plus or minus units can mean that either the data is moving towards or away from a stage 29 shape. When we look at both figure 12 and 13 together, we notice that for the frontonasal mass and maxillary prominence, the stage 29 data points are negative to the stage 20-28 data points. In

contrast, for the lateral nasal prominence and mandibular prominence, the stage 29 data points are positive relative to the stage 20-28 data points. Therefore, the mean wireframe for the frontonasal mass and maxillary prominence are closer to stage 20-28 data points, and +10 Mahalanobis units is transitioning towards stage 20-28. Meanwhile, the mean wireframe for the lateral nasal prominence is closer to stage 24-28 data points, and the mandibular prominence is closer to stage 20-28 data points, and +10 Mahalanobis units is transitioning towards a stage 29 shape

All facial prominences undergo a significant change in shape from the mean when comparing Mahalanobis and Procrustes distances amongst predefined groups (Table 6). Note that we only calculated variability in CV1, and variations along one canonical variate are statistically uncorrelated with variation along another canonical variate. However since CV1 covers the largest degree of variation, it is unnecessary to make such statistical calculations for the other CVs.

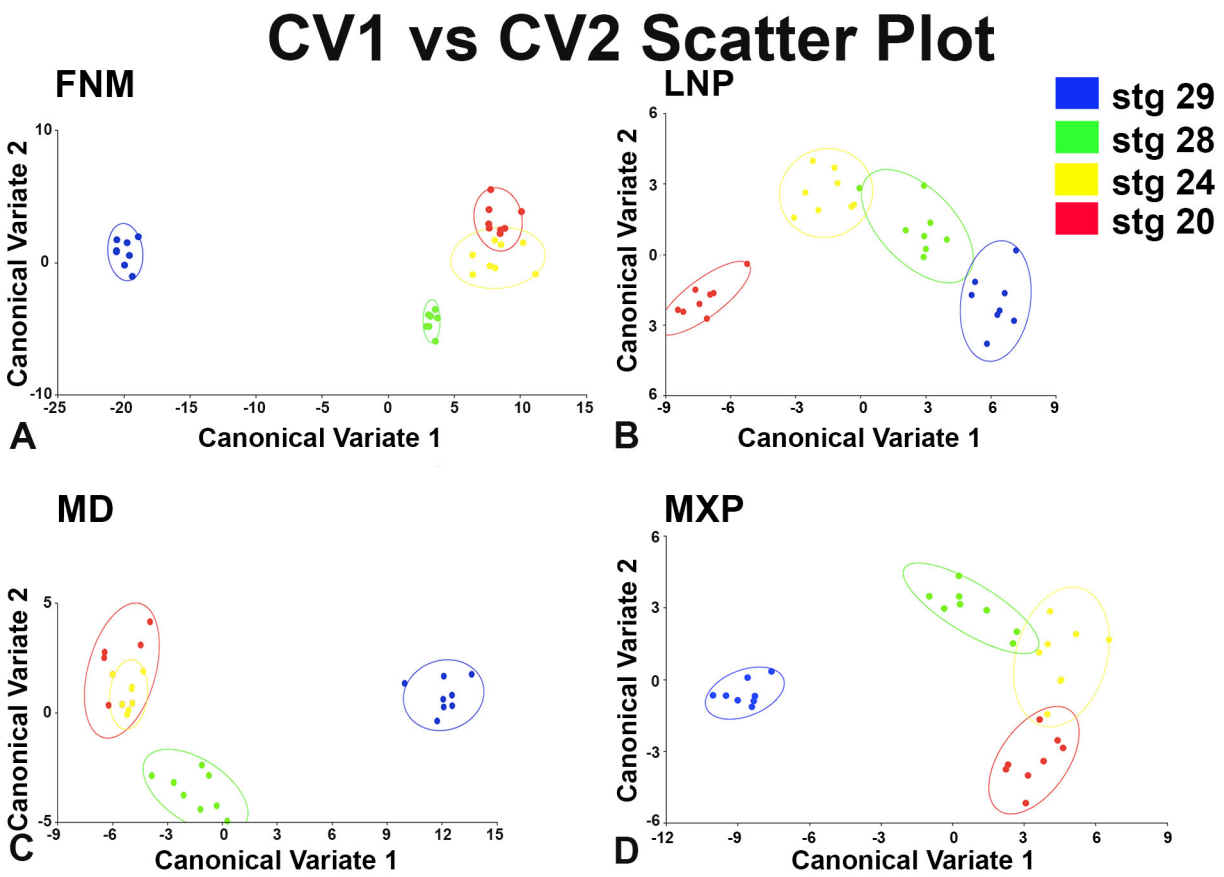

Figure 13– CVA – CV1 vs CV2
Graphical scatter plot output of the Canonical variate analysis of each of the individual facial prominences. CV1 is compared against CV2 as it contains the greatest amount of variability in the data set, and is most useful in identifying relationships between samples. Stage 20 – red, Stage 24 – yellow, Stage 28 – green, Stage 29 – blue. The centroid/consensus shape is at 0,0. The scale is measured in 10 units of Mahalanobis distance. A – CV1 vs CV2 of frontonasal mass. B – CV1 vs CV2 of lateral nasal prominence. C – CV1 vs CV2 of the mandibular prominence. D – CV1 vs CV2 of the maxillary prominence.

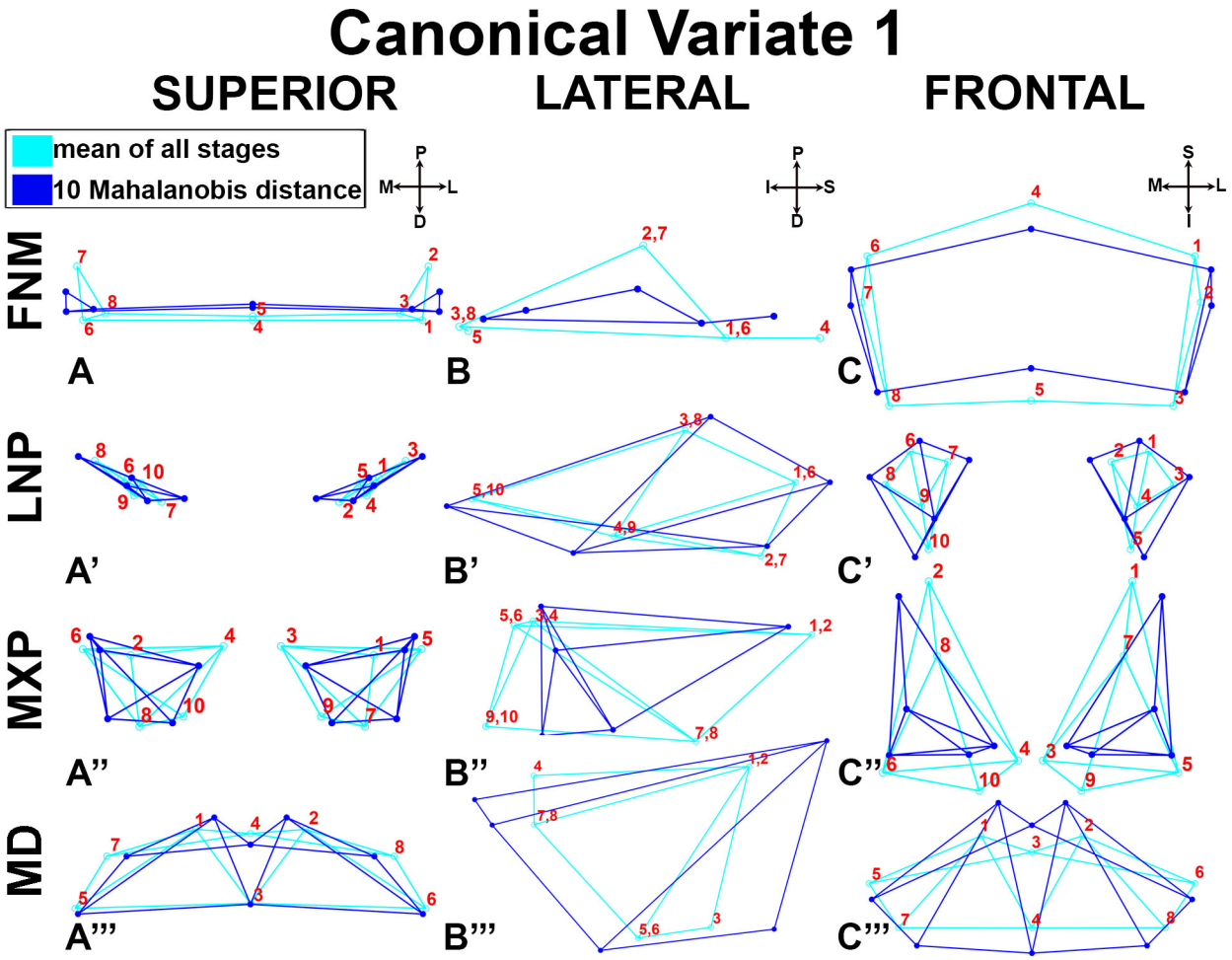

Figure 14 – CVA – Wireframe graph of CV1
CV1 of the individual facial prominences along the superior, lateral, and frontal plane. Light blue is the mean/consensus shape. The navy blue is +10 Mahalanobis units away from the mean. The blue dots and the red numbers indicate the landmarks chosen for each individual facial prominence. Landmark identifiers are only shown on the mean shape, and their change in location is interpolated onto the navy blue wireframe shape. Axes: D – distal, I – inferior, L – lateral, M – mesial, P – proximal, S – superior.

A. CVA - FRONTONASAL MASS			
Canonical Variates	**Eigenvalues**	**% Variance**	**Cumulative %**
1	155.818	**93.6**	93.6
2	8.83504	5.3	98.9
3	1.90314	1.1	100.0
Mahalanobis distances among groups:			
	20	**24**	**28**
24	4.48		
28	9.20	7.49	
29	28.37	28.29	23.79
Procrustes distances among groups:			
	20	**24**	**28**
24	0.11		
28	0.20	0.14	
29	0.48	0.44	0.36
B. CVA – LATERAL NASAL PROMINENCE			
Canonical Variates	**Eigenvalues**	**% Variance**	**Cumulative %**
1	28.620	**82.2**	82.2
2	4.502	12.9	95.1
3	1.700	4.9	100.0
Mahalanobis distances among groups:			
	20	**24**	**28**
24	7.35		
28	10.43	5.46	
29	13.48	9.09	5.52
Procrustes distances among groups:			
	20	**24**	**28**
24	0.07		
28	0.10	0.06	
29	0.16	0.11	0.08
B. CVA – MAXILLARY PROMINENCE			
Canonical Variates	**Eigenvalues**	**% Variance**	**Cumulative %**
1	31.174	**81.0**	81.0
2	6.130	15.9	96.9
3	1.182	3.1	100.0
Mahalanobis distances among groups:			
	20	**24**	**28**
24	4.96		
28	6.89	5.04	
29	12.50	13.41	10.25

B. CVA – MAXILLARY PROMINENCE continued			
Procrustes distances among groups:			
	20	**24**	**28**
24	0.08		
28	0.16	0.11	
29	0.34	0.31	0.21
D. CVA – MANDIBULAR PROMINENCE			
Canonical Variates	**Eigenvalues**	**% Variance**	**Cumulative %**
1	58.375	**91.1**	91.1
2	5.133	8.0	99.1
3	0.556	0.9	100.0
Mahalanobis distances among groups:			
	20	**24**	**28**
24	2.25		
28	6.86	5.88	
29	17.63	17.22	14.24
Procrustes distances among groups:			
	20	**24**	**28**
24	0.07		
28	0.18	0.14	
29	0.43	0.41	0.30

Table 7 – Canonical Variate Analysis
CVA of the individual facial prominences showing the number of canonical variates, the corresponding eigenvalues, the % variance, and the cumulative % of total variance.
A – CVA of the frontonasal mass reveals 3 canonical variates that account for 100% of the variance in shape. Canonical variate 1 (CV1) alone accounts for 93.6% of the shape variation. Mahalanobis and Procrustes distances amongst groups reveal greatest group differences between stage 29 and stages 20, 24, and 28. Stages 20, 24, and 28 are quite similar
B – CVA of the lateral nasal prominence reveals 3 canonical variates that account for 100% of the variance in shape. Canonical variate 1 (CV1) alone accounts for 82.2% of the shape variation. Mahalanobis and Procrustes distances amongst groups reveal group differences between stage 20, 24, 28, and 29 are quite similar.
C – CVA of maxillary prominence reveals 3 canonical variates that account for 100% of the variance in shape. Canonical variate 1 (CV1) alone accounts for 81.0% of the shape variation. Mahalanobis and Procrustes distances amongst groups reveal greatest group differences between stage 29 and stages 20, 24, and 28. Stages 20, 24, and 28 are quite similar.
D – CVA of the mandibular prominence reveals 3 canonical variates that account for 100% of the variance in shape. Canonical variate 1 (CV1) alone accounts for 91.1% of the shape variation. Mahalanobis and Procrustes distances amongst groups reveal greatest group differences between stage 29 and stages 20, 24, and 28. Stages 20, 24, and 28 are quite similar

3.9 Discriminant Function Analysis

Discriminant function analysis (DFA) is a multivariate test similar to the CVA. Groups are defined a priori, but unlike a CVA, only two groups are included in the analysis. In order to tease apart changes between specific landmarks at different stages, DFA allows us to compare specific groups of interest, unlike the CVA which compares all the groups in a single analysis. We were particularly interested in using DFA to determine why there was such a big change in shape of the frontonasal mass and mandibular prominence between stages 28 and 29.

We have chosen to display the results of the DFA in two formats: wireframe output, and a text output. The wireframe output compares the mean/consensus wireframe shape between the two predetermined groups (Figures 14, 15, 16, 17). The text output reveals the difference between means of the individual facial prominences in respect to Procrustes distance, Mahalanobis unit, T-square, and p-value (Table 8,9,10,11).

When comparing stages 20 and 24, the wireframe graphs show minimal shape change (Figure 14). The time from stage 20 to 24 is approximately 24 hours. Most of the change, though minimal, is visible along the lateral plane. Most notably, for the frontonasal mass, the lateral aspects are flexing distally, and the midline is flexing proximally (Figure 14A). The lateral nasal prominences are rotating medially (Figure 14C'), the maxillary prominence is converging superior-inferiorly (Figure 14B"), and the mandibular prominence is converging proximo-distally (Figure 14B"'). Table 8 reveals that there is statistically significant shape differences between a stage 20 and stage 24 frontonasal mass and lateral nasal prominence.

When comparing stage 24 and 28, the wireframe graph shows increased shape changes for all facial prominences (Figure 15). The time from stage 24 to 28 is approximately 36 hours.

The shape change can be observed in all three planes of space. The frontonasal mass is expanding superior-inferiorly (Figure 15B), and the inferior-lateral margins are beginning to converge medially (Figure 15C). The lateral nasal prominence is rotating laterally (Figure 15A'), and converging superior-inferiorly (Figure 15B'). The maxillary prominence has begun to converge proximo-distally (Figure 15B'') and the posterior aspect is rotating laterally (Figure 15A'') and the anterior portion is rotating medially (Figure C"). Lastly, the mandibular prominence has expanded proximo-distally and superior-inferiorly (Figure 15A"', B"'). The tips are also transitioning proximally (Figure 15B"'). Table 9 indicates that there is statistically significant shape change for the frontonasal mass, lateral nasal prominence, and mandibular prominence as it transitions from stage 24 to stage 28.

When comparing the most divergent stages, stage 28 and 29, the wireframe graph shows considerable differences in shape for all facial prominences (Figure 16). The time from stage 28 and 29 is approximately 12 hours. The shape change is markedly visible in all three planes of space for all facial prominences. In the frontonasal mass, there is a significant transformation in shape as there is considerable expansion superior-inferiorly (Figure 16B,C) and convergence medial-laterally (Figure 16A,C). The frontonasal mass also depresses distally as the depth of the nasal pits deepen proximally (landmarks 2,7, Figure 16A). For the lateral nasal prominence, there is convergence proximo-distally (Figure 16B'), and lateral rotation (Figure 16C'). In the maxillary prominence, there is expansion proximo-distally and superior-inferiorly (Figure 16B"), as the superior portion is rotating medially. Lastly, the mandibular prominence is dramatically expanding superior-inferiorly (Figure 16B"', C"'), and converging proximo-distally (Figure 16B"'). Table 10 reveals statistically significant shape changes for all facial prominences.

When comparing stage 20 and 29, the wireframe graphs show considerable shape change for all facial prominences (Figure 17). The time for a chick embryo to transition from stage 20 and 29 is approximately 72 hours. The shape change is visible in all three planes of space as mentioned previously in their stage by stage breakdown. To summarize, the frontonasal mass converges mediolaterally (Figure 17A,C), and expands superior-inferiorly (Figure 16B,C), while it depresses distally (Figure 17A), and the nasal pits deepen proximally (Figure 17A). For the lateral nasal prominence, it expands superior-inferiorly and proximo-distally (Figure 17B',C'), as the inferior aspect rotates laterally (Figure 17C'). In the maxillary prominence, there is expansion superio-inferiorly, proximo-distally, and translation medially (Figure 17A",B",C") and rotation of the superior aspect medially (Figure 17C"). Lastly, in the mandibular prominence, there is convergence medio-laterally (Figure 17A"') and proximo-distally (Figure 17B"'), and significant expansion superior-inferiorly (Figure 17B"'). The tips of the mandibular prominence also rotate proximally (landmark1,2, Figure 17B"'). Table 11 reveals that there is statistically significant differences between a stage 20 and stage 29 shape amongst all the facial prominences.

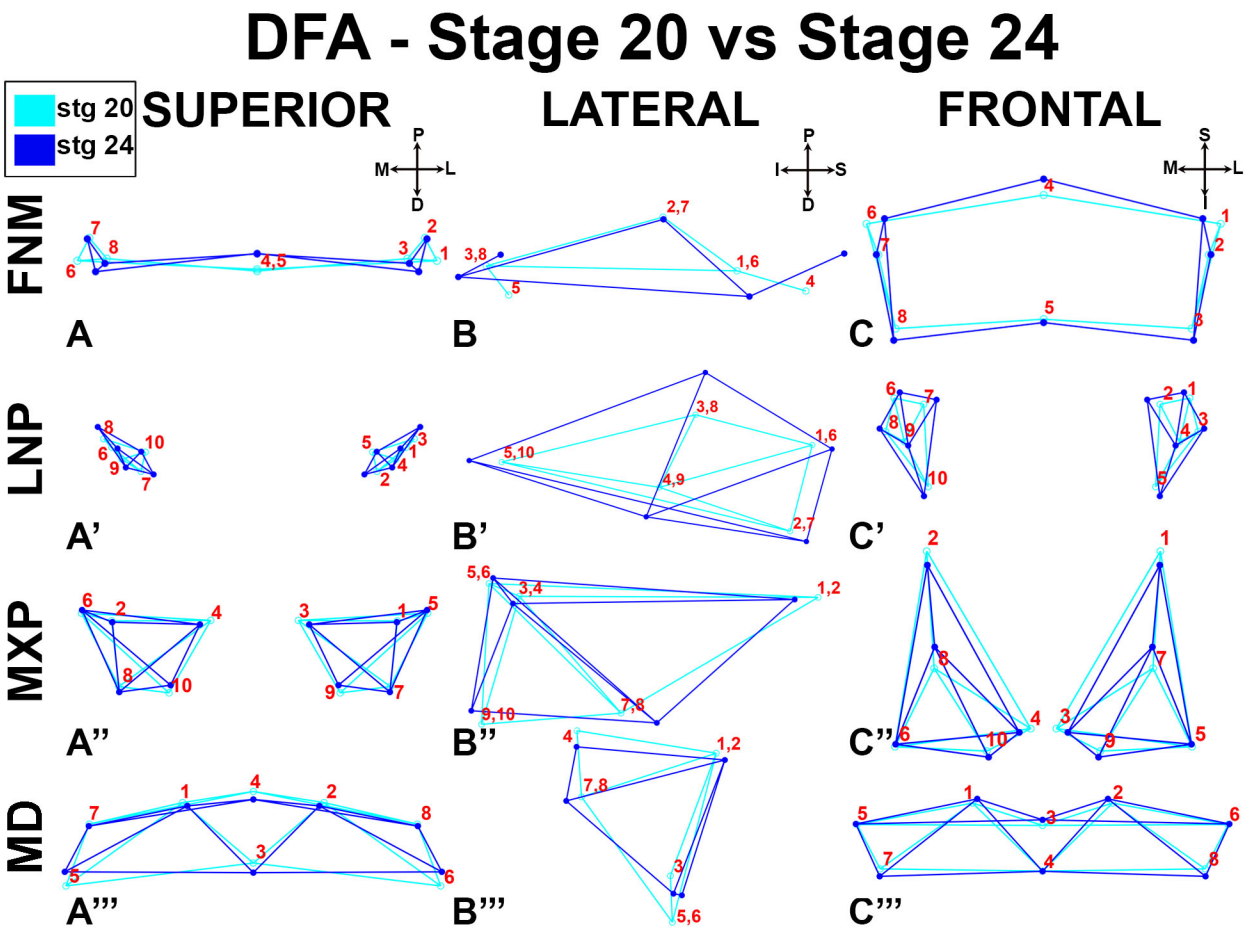

Figure 15 – DFA – Stage 20 to 24
Wireframe graph of mean stage 20 shape compared against mean stage 24 shape of all facial prominences along the superior, lateral, and frontal plane. Light blue is the mean/consensus shape of stage 20, and the navy blue is the mean/consensus shape of stage 24. The blue dots and the red numbers indicate the landmarks chosen for each individual facial prominence. Landmark identifiers are only shown on the stage 20 shape, and their change in location is interpolated onto the navy blue wireframe shape. Axes: D – distal, I – inferior, L – lateral, M – mesial, P – proximal, S – superior.

Discriminant Function Analysis STAGE 20 to STAGE 24				
Difference between means:	**FRONTONASAL MASS**	**LATERAL NASAL**	**MAXILLARY PROMINENCE**	**MANDIBULAR PROMINENCE**
Procrustes distance:	0.11	0.07	0.08	0.07
Mahalanobis distance:	4.75	24.56	5.05	2.03
T-square:	90.39	2413.23	101.92	16.56
P-value (parametric):	0.0448	0.0006	0.1801	0.6408

Table 8 – DFA – Stage 20 to Stage 24
DFA comparing the means of the stage 20 and stage 24 shape of the individual facial prominences. The text output reveals the difference between means of the individual facial prominences in respect to Procrustes distance, Mahalanobis unit, T-square, and associated p-value.

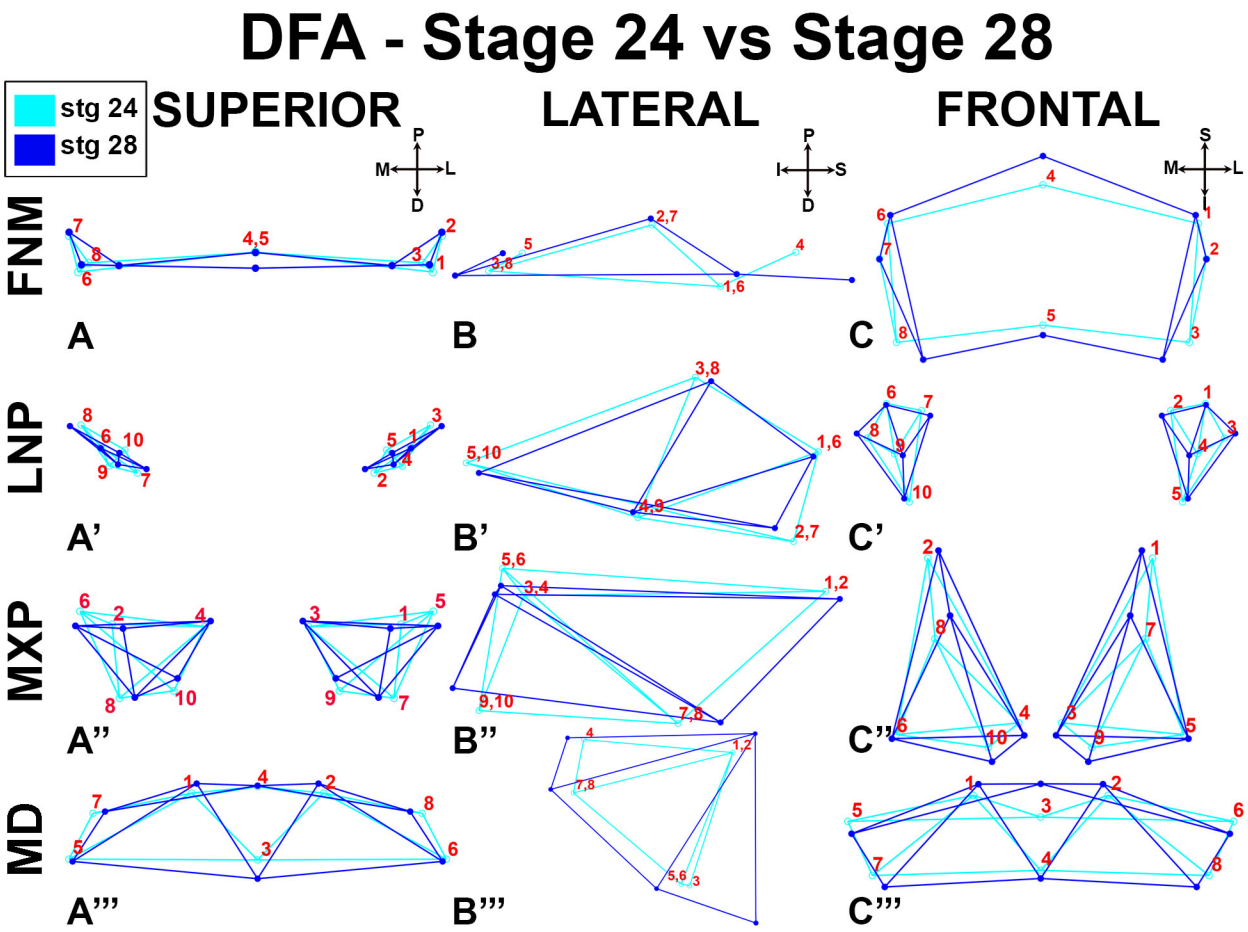

Figure 16 – DFA – Stage 24 to 28
Wireframe graph of mean stage 24 shape compared against mean stage 28 shape of all facial prominences along the superior, lateral, and frontal plane. Light blue is the mean/consensus shape of stage 24, and the navy blue is the mean/consensus shape of stage 28. The blue dots and the red numbers indicate the landmarks chosen for each individual facial prominence. Landmark identifiers are only shown on the stage 24 shape, and their change in location is interpolated onto the navy blue wireframe shape. Axes: D – distal, I – inferior, L – lateral, M – mesial, P – proximal, S – superior.

Discriminant Function Analysis STAGE 24 to STAGE 28				
Difference between means:	**FRONTONASAL MASS**	**LATERAL NASAL**	**MAXILLARY PROMINENCE**	**MANDIBULAR PROMINENCE**
Procrustes distance:	0.14	0.06	0.11	0.14
Mahalanobis distance:	10.31	14.68	6.16	8.37
T-square:	425.57	861.54	152.01	280.20
P-value (parametric):	0.0008	0.0044	0.0983	0.0025

Table 9 – DFA – Stage 24 to 28
DFA comparing the means of the stage 24 and stage 28 shape of the individual facial prominences. The text output reveals the difference between means of the individual facial prominences in respect to Procrustes distance, Mahalanobis unit, T-square, and associated p-value.

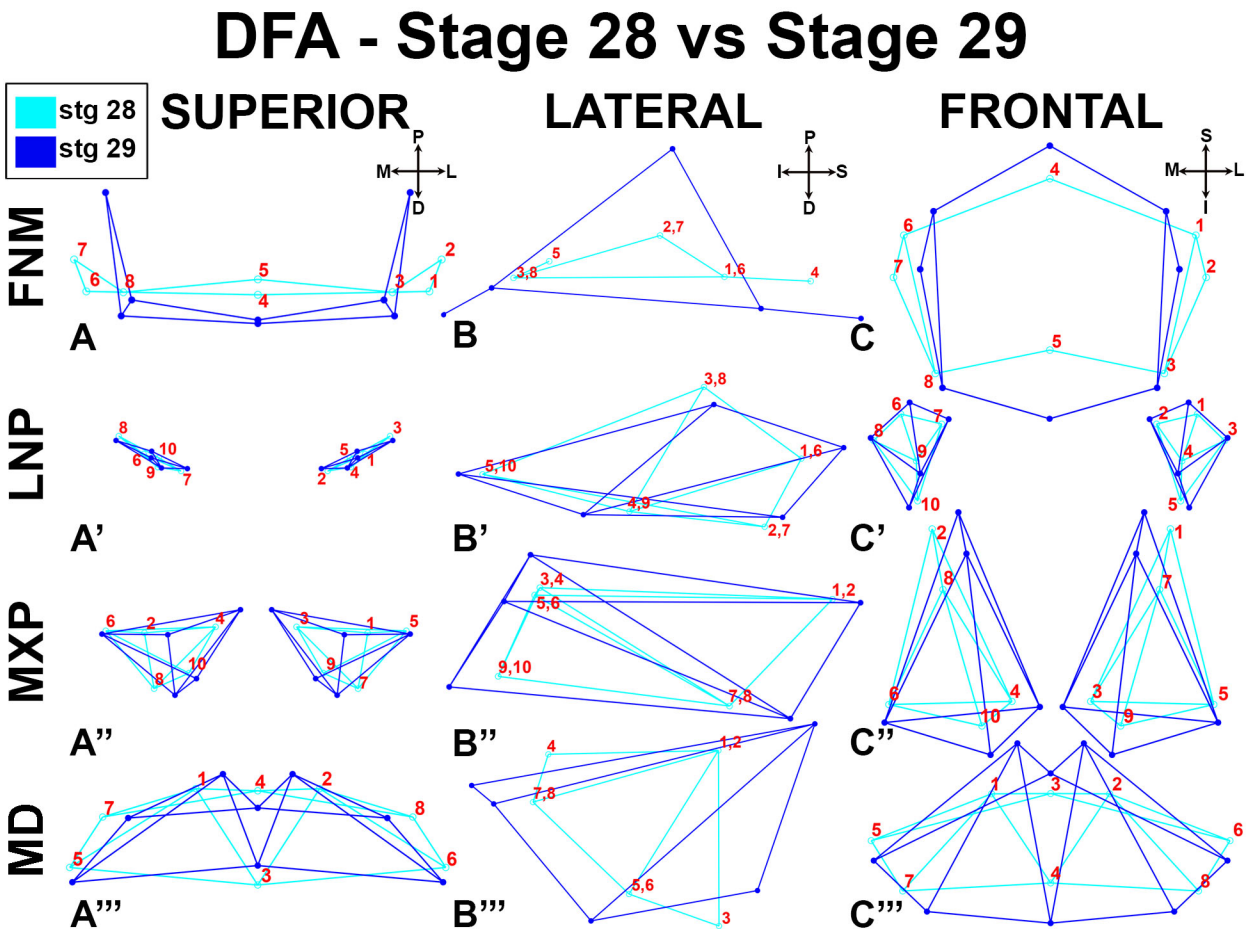

Figure 17 – DFA – Stage 28 to 29
Wireframe graph of mean stage 28 shape compared against mean stage 29 shape of all facial prominences along the superior, lateral, and frontal plane. Light blue is the mean/consensus shape of stage 28, and the navy blue is the mean/consensus shape of stage 29. The blue dots and the red numbers indicate the landmarks chosen for each individual facial prominence. Landmark identifiers are only shown on the stage 28 shape, and their change in location is interpolated onto the navy blue wireframe shape. Axes: D – distal, I – inferior, L – lateral, M – mesial, P – proximal, S – superior.

Discriminant Function Analysis: STAGE 20 to STAGE 29				
Difference between means:	**FRONTONASAL MASS**	**LATERAL NASAL**	**MAXILLARY PROMINENCE**	**MANDIBULAR PROMINENCE**
Procrustes distance:	0.48	0.16	0.34	0.43
Mahalanobis distance:	44.41	42.93	133.77	37.88
T-square:	7889.10	7373.24	71582.28	5738.84
P-value (parametric):	<.0001	<.0001	<.0001	<.0001

Table 10 – DFA – Stage 28 to 29
DFA comparing the means of the stage 28 and stage 29 shape of the individual facial prominences. The text output reveals the difference between means of the individual facial prominences in respect to Procrustes distance, Mahalanobis unit, T-square, and associated p-value.

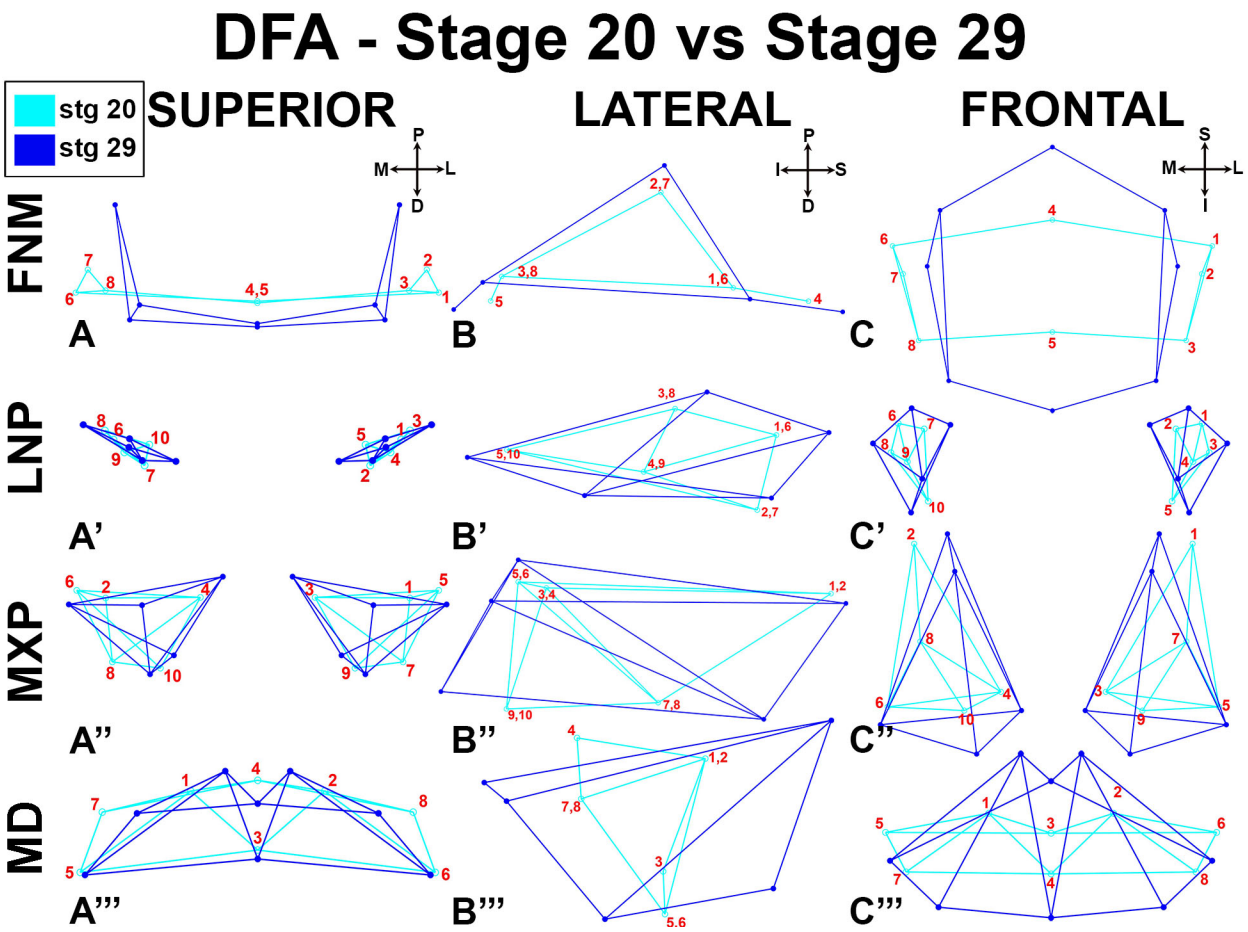

Figure 18 – DFA – Stage 20 to 29
Wireframe graph of mean stage 20 shape compared against mean stage 29 shape of all facial prominences along the superior, lateral, and frontal plane. Light blue is the mean/consensus shape of stage 20, and the navy blue is the mean/consensus shape of stage 29. The blue dots and the red numbers indicate the landmarks chosen for each individual facial prominence. Landmark identifiers are only shown on the stage 20 shape, and their change in location is interpolated onto the navy blue wireframe shape. Axes: D – distal, I – inferior, L – lateral, M – mesial, P – proximal, S – superior.

Discriminant Function Analysis: STAGE 20 to STAGE 29				
Difference between means:	**FRONTONASAL MASS**	**LATERAL NASAL**	**MAXILLARY PROMINENCE**	**MANDIBULAR PROMINENCE**
Procrustes distance:	0.48	0.16	0.34	0.43
Mahalanobis distance:	44.41	42.93	133.77	37.88
T-square:	7889.10	7373.24	71582.28	5738.84
P-value (parametric):	<.0001	<.0001	<.0001	<.0001

Table 11 – DFA – Stage 20 to 29
DFA comparing the means of the stage 20 and stage 29 shape of the individual facial prominences. The text output reveals the difference between means of the individual facial prominences in respect to Procrustes distance, Mahalanobis unit, T-square, and associated p-value.

Chapter 4: Discussion

4.1 Correlation between cell cycle length and periods of most significant morphogenetic change

Up until this point, I have focused mainly on the Hamburger and Hamilton staging criteria when discussing my results. It is interesting to note that the intervals between stages 20-24, 24-28 are each 24h of incubation. However the interval between stage 28 and 29 is only 12 hours. The rapidity with which significant shape changes occurs is very striking especially when compared to cell cycle times in the chicken embryo face. A detailed series of studies using tritiated thymidine to analyze the length of each phase of the cell cycle in the face was carried out by R. Minkoff (Bailey et al., 1988; Minkoff, 1984; Minkoff, 1991; Minkoff and Kuntz, 1977; Minkoff and Kuntz, 1978). He is the only author to calculate cell cycle time in the face. His main findings were that for the stage 24-26 maxillary prominence, the mean cell cycle time for the mesenchyme was 12 hours (Minkoff, 1984). In chondrogenic regions, mean cell cycle time was much longer (18h) and many cells had exited the cell cycle. Extrapolating to other regions of the face is reasonable based on similarity of the local environment, however it is possible that in the frontonasal mass, mandibular and lateral nasal prominences, the areas where cartilage is forming will have lower cell cycle times. Based on the maxillary data there should be approximately 2 cell divisions between stages 20 and 24, 24 and 28. This would quadruple cell number and accounts for much of the volumetric increase observed between these stages. Between stages 20 and 28, the frontonasal mass has increased six times in volume, the maxillary and mandibular prominence have increased thirteen times in volume, and the lateral nasal prominence has increased the most by twenty-four times in volume when compared to their stage 20 volumes.

These data fit well with the cell doubling times and suggest that most of the subtle shape changes that occur during this period could be explained by regional differences in cell proliferation. Within the frontonasal mass, highest proliferation indices are measured in the areas adjacent to the nasal processes (Minkoff and Kuntz, 1977). The centre of the frontonasal mass has relatively low proliferation especially at stage 28 when the prenasal cartilage begins to differentiate (MacDonald et al., 2004; McGonnell et al., 1998; Szabo-Rogers et al., 2008). The maxillary prominence goes through a longer period of time (between stages 20 to 28, 72h) where minimal shape changes are observed as supported in the PCA and CVA. In addition, the DFA of the maxillary prominence between stages 20 to 24, and stage 24 to 28, reveals that there is no statistically significant difference in shape. One would predict that with such even morphogenesis, there would also be radially symmetric proliferation in the maxillary mesenchyme. Detailed analysis of proliferation in sub-regions of the chicken maxillary prominence between stages 24-29 was carried out recently by the Richman Lab (Abramyan et al., 2014). Proliferation was initially even throughout the maxillary prominence at stage 24. As the chick embryos advanced in development, polarized differences in proliferation patterns appeared (Abramyan et al., 2014). The most critical time where major regional differences occur is between stages 28 and 29 which correlates nicely with our PCA, CFA and DFA analyses.

However between stages 28 and 29 there would have only been time for a single cell division or doubling of cell number. It is very striking that between these two stages, (days 5.0-5.5), all facial prominences are statistically significant from their respective stage 28 shape. From the wireframe graph of these two stages, one can visualize the gross differences between a stage 28 and stage 29 frontonasal mass, maxillary prominence, and mandibular prominence. The frontonasal mass undergoes significant convergence mediolaterally, extension superior-

inferiorly, and proximodistaly, and the tip of the beak begins to rotate distally towards the mandibular prominence. The mandibular prominence extends superior-inferiorly and converges proximodistally, while the tips begin to turn upward to contact the converging and distally rotating frontonasal mass. At stage 29 the beak begins to project out from the rest of the head. Only the frontonasal mass and mandibular prominence undergo convergent extension relative to the position of our landmarks, and it is in these regions that we predict other mechanisms in addition to cell proliferation that must be contributing to the rapid changes in shape.

Other cellular mechanisms that could be driving the shape changes include individual cell shape changes in one particular axis, oriented cell division in one axis, intercalation or stacking of cells in one axis and directed cell migration. The best data on such mechanisms in the face was collected on the mouse secondary palate between E12.5 and 14.5 when fusion occurred. In the paper by Economou et al. in 2013 (Economou et al., 2013), they identified that posterior elongation of mice palatal mesenchyme was 60% attributed to cell proliferation, and 40% to a combination of cellular elongation, intercalation, oriented cell division, and rearrangements. No specific molecules were identified in this study that accounted for these changes. In a study on the frontonasal mass, Li et al., (Li et al., 2013) demonstrated that in normal cells, orientation of the Golgi body matched the direction of facial prominence outgrowth. One of the signals that regulates both proliferation and polarity is FGF. Ectopic FGF signaling in treated embryos demonstrated decreased cell proliferation as well as a randomized orientation of facial mesenchymal cells (Li et al., 2013). The Richman Lab has also shown that FGF signaling is critical for regulating regional cell proliferation in the lateral edges of the frontonasal mass (Szabo-Rogers et al., 2008). More recently detailed studies on WNT11 have revealed that directional cell migration can be induced by WNT11 in the maxillary prominence (Geetha-

Loganathan et al., 2014). In addition when WNT11 is knocked down, cells become shorter and appear to be more oriented. WNT11 is also required for cell proliferation so there are dual roles for this growth factor in regulating morphogenesis. Future studies on signaling in facial mesenchyme should be focused between stages 28 and 29 and in particular on the frontonasal and mandibular mesenchyme.

4.2 Major shape changes in the face between stages 28 and 29 can be partially attributed to onset of chondrogenesis and lip fusion

Alongside the dramatic change within the frontonasal mass and mandibular prominence is the exiting of a group of cells from the cell cycle to form cartilage condensations. It is not just in the bird that timing of differentiation coincides with major shape changes, but also in the human (Diewert and Lozanoff, 1993a). Landmarks were identified on photographs of midsagittal sections of human embryos at stages 16 to 19 during primary palate formation. Analysis determined that shape change was most prominent in the posterior cranial and orofacial region at this time. This indicated an interplay between cranial and midfacial regions, and their impact and role during primary palate formation.

Fusion is also occurring in the upper face between the frontonasal mass, lateral nasal prominence and maxillary prominence between stages 28 and 29. It is clear that if cell signaling in the FGF(Li et al., 2013; Szabo-Rogers et al., 2008), BMP (Ashique et al., 2002a) or WNT pathway (Geetha-Loganathan et al., 2014) is disrupted, cleft lip will result. Mainly proliferation and cell apoptosis have been studied as the mechanisms, but my work suggests that more subtle changes in facial prominence shape could also play a role. If the maxillary prominence is prevented from elongating in the cranial-caudal axis due to increased levels of WNT11, cleft lip

occurs (Geetha-Loganathan et al., 2014). The shape differences were not analyzed using geometric morphometrics in this study.

Most recently, Young et al., in 2014 (Young et al., 2014) attempted to explain the presence of a conserved stage of events in amniote facial development across major amniotic lineages. They attempted to compare multiple amniotes by performing geometric morphometrics on surface landmarks of the maxillary and frontonasal prominences. A major divergence in shape and growth was identified post-fusion. Interestingly, they induced clefts in some chicken embryos and found that the presence or absence of clefting in the primary palate changed the embryo group into a non-avian growth trajectory. In 2007, Young et al. (Young et al., 2007) used geometric morphometrics to explain variations in midface morphology for normal and cleft lip mouse embryos. Frontal and lateral landmarks were identified on 2D photographs of early and late embryos, and analysis determined that the presence of clefting was due to a combination of discrepancy in midface shape and cell surface defects. Cleft-susceptible mice tended to have reduced contact area between the underdeveloped maxillary prominences.

The adoption of 3D GMM for the analysis of face shape in chicken and mouse mutants at early stages prior to overt clefts will provide new insights into the understanding of the pathophysiology of clefting.

4.3 Technical and Biological Variation

A major obstacle to reliably determine quantitative shape changes is to overcome errors imposed by technical variation and biological variation. Technical variation within my thesis includes my expertise in landmarking and segmenting the facial prominences. Segmenting facial prominences was a challenge because the internal surfaces did not interface with air. To

reduce error, I traced the same prominence at different planes to accurately capture as much of the prominence as possible. However, I did not repeat the segmentation for each facial prominence therefore the variation I observed was a combination of biological and technical. Although variation might have been higher than desirable, it was possible to clearly distinguish the different stages of embryos for most of the facial prominences even after regression on centroid size. If anything could be improved, it might be to repeat segmentation on the stage 20 facial prominences and then to create an average isosurface from the technical replicates prior to applying landmarks. Such an overlay is possible within the Landmark program.

Landmarking improved over time as margins and features became more readily identifiable in the older stages of embryos. I did perform technical replicates of the maxillary prominence within and between groups of stage 20 and 24 embryos which are the most difficult to distinguish. Even these challenging specimens could be reliably landmarked; therefore, it is reasonable to assume the mandibular, frontonasal and lateral nasal landmarks are reliable and reproducible.

Biological variation can be due to variation in the rate of growth of chicken embryos. Variations in form and development are intrinsic within a species. As we saw, the growth curve was exponential for most facial prominences. Thus there will be a chance that one stage 20 is perhaps more advanced than another. In addition, there could be variability from the egg source with respect to freshness of the eggs, storage methods, and time from laying to delivery. We did minimize biological variation by synchronizing the embryos at stage 15 using somite numbers, therefore the variation is mostly due to actual shape differences in between embryos as shown in our regression analysis.

4.4 Limitations

A scientific limitation of our study is the approach to finding relationships between mathematical morphometrics and biological changes. With PCA, PC1 is the best fitting line through the data, and does not represent any particular stage well. PC2 is the direction orthogonal to PC1 that describes most of the remaining variation around the sample mean. There may be a biological factor that explains PC1, but there need not be. PCs might be an average effect of multiple factors, especially if multiple groups are analyzed. In addition, PCs are constrained to be orthogonal, but biological factors are not restricted to the same constraints. This is why PCs can be an average effect of multiple factors, and not be explicable in biological terms. The axes are mathematical constructs, and are difficult to explain biologically. PCs do not account for relationships between groups, as it analyzes variation among individuals, as if they were all a single group. By performing a CVA, we labelled the stages a priori, such that we looked at between-group variations instead. DFA is useful, as it allows us to compare between two stages independently. However, the principal of PCA, CVA, and DFA reveals that only differences if present are identifiable, and is more to further hypothesis testing as these mathematical methods do not necessarily coincide with biological factors or processes.

A technical limitation of our study is the small sample size, which meant that we could not place more than 5 landmarks. The limitation on landmarks may have meant we missed important features of the facial prominences. All results should be interpreted with caution, and need to be reevaluated with a larger data set.

4.5 Future Directions and other applications

A specific application of this research is that we now know where to focus our efforts for single cell analysis. Areas of the face that would be interesting to focus on would be areas of extensive shape rearrangement including the frontonasal mass and the mandibular prominence. It would also be interesting to look more specifically at the transition period between stage 28 and 29. This would help explain the underlying processes necessary for the rapid and dramatic rearrangement seen in the study.

A fascinating future direction would be to test the role of extrinsic versus intrinsic factors that control frontonasal mass shape, especially between stages 28 and 29. For example the expansion of the forebrain is considerable, and eventually the frontonasal mass becomes tucked under the telencephalic vesicles. The brain growth might be more rapid than frontonasal growth leading to relative, but narrowing of the facial midline. The eyes also undergo a huge expansion in the chicken embryo between stage 20 and 29. It is possible that the eyes displace the frontonasal mass and compress it in the midline. Interestingly, a previous study in which the right eye was enucleated at stage 12 showed that the upper beak still formed normally, although it was deviated to the right side (Thompson et al., 2010. Thus it would appear that the frontonasal mass still narrowed normally, in the absence of eye influences. It is certainly feasible to grow the face in isolation from the rest of the head in an organ culture system over the period of time when narrowing is taking place. This experiment would more clearly distinguish the role of intrinsic versus extrinsic forces in facial narrowing.

In summary, GMM is a sensitive approach to determine the earliest changes in shape that can occur before differentiation of tissues can be identified. By landmarking and segmenting out the area of interest or modulation, one can mathematically identify if a statistically significant

difference is present, and not rely solely on qualitative observations. This also helps in identifying whether the difference seen is because of natural growth, or a true effect of the modulation. Other studies have used these methods to measure shape changes in differentiated skulls and embryos (Attanasio et al., 2013; Hallgrimsson et al., 2004; Young et al., 2014; Young et al., 2007). Ours is the only one to have applied geometric morphometrics to individual facial prominences, and has provided a very useful baseline against which to compare treated embryos. In the future we will use GMM to point towards the most likely cellular mechanisms involved in abnormal facial morphogenesis, and will direct the course of subsequent molecular studies.

Bibliography

Abramyan, J., Leung, K. J. and Richman, J. M. (2014). Divergent palate morphology in turtles and birds correlates with differences in proliferation and BMP2 expression during embryonic development. *J Exp Zool B Mol Dev Evol* **322**, 73-85.

Abzhanov, A., Protas, M., Grant, B. R., Grant, P. R. and Tabin, C. J. (2004). Bmp4 and morphological variation of beaks in Darwin's finches. *Science* **305**, 1462-5.

Abzhanov, A., Rodda, S. J., McMahon, A. P. and Tabin, C. J. (2007). Regulation of skeletogenic differentiation in cranial dermal bone. *Development* **134**, 3133-44.

Aldur, M. M. (2005). Creating computer aided 3D model of spleen and kidney based on Visible Human Project. *Saudi Med J* **26**, 51-6.

Ashique, A. M., Fu, K. and Richman, J. M. (2002a). Endogenous bone morphogenetic proteins regulate outgrowth and epithelial survival during avian lip fusion. *Development* **129**, 4647-60.

Ashique, A. M., Fu, K. and Richman, J. M. (2002b). Signalling via type IA and type IB bone morphogenetic protein receptors (BMPR) regulates intramembranous bone formation, chondrogenesis and feather formation in the chicken embryo. *Int J Dev Biol* **46**, 243-53.

Attanasio, C., Nord, A. S., Zhu, Y., Blow, M. J., Li, Z., Liberton, D. K., Morrison, H., Plajzer-Frick, I., Holt, A., Hosseini, R. et al. (2013). Fine tuning of craniofacial morphology by distant-acting enhancers. *Science* **342**, 1241006.

Bailey, L. J., Minkoff, R. and Koch, W. E. (1988). Relative growth rates of maxillary mesenchyme in the chick embryo. *J Craniofac Genet Dev Biol* **8**, 167-77.

Barlow, A. J. and Francis-West, P. H. (1997). Ectopic application of recombinant BMP-2 and BMP-4 can change patterning of developing chick facial primordia. *Development* **124**, 391-8.

Beckmann, F., Bonse, U., Busch, F. and Gunnewig, O. (1997). X-ray microtomography (microCT) using phase contrast for the investigation of organic matter. *J Comput Assist Tomogr* **21**, 539-53.

Belloni, E., Muenke, M., Roessler, E., Traverso, G., Siegel-Bartelt, J., Frumkin, A., Mitchell, H. F., Donis-Keller, H., Helms, C., Hing, A. V. et al. (1996). Identification of Sonic hedgehog as a candidate gene responsible for holoprosencephaly. *Nat Genet* **14**, 353-6.

Benouaiche, L., Gitton, Y., Vincent, C., Couly, G. and Levi, G. (2008). Sonic hedgehog signalling from foregut endoderm patterns the avian nasal capsule. *Development* **135**, 2221-5.

Boell, L., Pallares, L. F., Brodski, C., Chen, Y., Christian, J. L., Kousa, Y. A., Kuss, P., Nelsen, S., Novikov, O., Schutte, B. C. et al. (2013). Exploring the effects of gene dosage on

mandible shape in mice as a model for studying the genetic basis of natural variation. *Dev Genes Evol* **223**, 279-87.

Bonse, U. and Busch, F. (1996). X-ray computed microtomography (microCT) using synchrotron radiation (SR). *Prog Biophys Mol Biol* **65**, 133-69.

Bookstein, F. L. (1991). Morphometric tools for landmark data : geometry and biology. Cambridge England ; New York: Cambridge University Press.

Brito, J. M., Teillet, M. A. and Le Douarin, N. M. (2006). An early role for sonic hedgehog from foregut endoderm in jaw development: ensuring neural crest cell survival. *Proc Natl Acad Sci U S A* **103**, 11607-12.

Chai, Y., Jiang, X., Ito, Y., Bringas, P., Jr., Han, J., Rowitch, D. H., Soriano, P., McMahon, A. P. and Sucov, H. M. (2000). Fate of the mammalian cranial neural crest during tooth and mandibular morphogenesis. *Development* **127**, 1671-9.

Cordero, D., Marcucio, R., Hu, D., Gaffield, W., Tapadia, M. and Helms, J. A. (2004). Temporal perturbations in sonic hedgehog signaling elicit the spectrum of holoprosencephaly phenotypes. *J Clin Invest* **114**, 485-94.

Couly, G., Creuzet, S., Bennaceur, S., Vincent, C. and Le Douarin, N. M. (2002). Interactions between Hox-negative cephalic neural crest cells and the foregut endoderm in patterning the facial skeleton in the vertebrate head. *Development* **129**, 1061-73.

Couly, G. F., Coltey, P. M. and Le Douarin, N. M. (1993). The triple origin of skull in higher vertebrates: a study in quail-chick chimeras. *Development* **117**, 409-29.

DeMyer, W. (1975). Median facial malformations and their implications for brain malformations. *Birth Defects Orig Artic Ser* **11**, 155-81.

Diewert, V. M. and Lozanoff, S. (1993a). Growth and morphogenesis of the human embryonic midface during primary palate formation analyzed in frontal sections. *J Craniofac Genet Dev Biol* **13**, 162-83.

Diewert, V. M. and Lozanoff, S. (1993b). A morphometric analysis of human embryonic craniofacial growth in the median plane during primary palate formation. *J Craniofac Genet Dev Biol* **13**, 147-61.

Dubourg, C., Bendavid, C., Pasquier, L., Henry, C., Odent, S. and David, V. (2007). Holoprosencephaly. *Orphanet J Rare Dis* **2**, 8.

Dürer, A. (1525). Underweysung der Messung, mit dem Zirckel unnd richt scheyt, in Linien ebnen unnd gantzen Corporen. Nuremberg: s.n.

Economou, A. D., Brock, L. J., Cobourne, M. T. and Green, J. B. (2013). Whole population cell analysis of a landmark-rich mammalian epithelium reveals multiple elongation mechanisms. *Development* **140**, 4740-50.

Fish, J. L., Sklar, R. S., Woronowicz, K. C. and Schneider, R. A. (2014). Multiple developmental mechanisms regulate species-specific jaw size. *Development* **141**, 674-84.

Foppiano, S., Hu, D. and Marcucio, R. S. (2007). Signaling by bone morphogenetic proteins directs formation of an ectodermal signaling center that regulates craniofacial development. *Dev Biol* **312**, 103-14.

Foster, F. S., Hossack, J. and Adamson, S. L. (2011). Micro-ultrasound for preclinical imaging. *Interface Focus* **1**, 576-601.

Geetha-Loganathan, P., Nimmagadda, S., Fu, K. and Richman, J. M. (2014). Avian Facial Morphogenesis is Regulated by JNK/PCP Wingless-Related (WNT) Signaling. *J Biol Chem*.

Gu, S., Jenkins, M. W., Watanabe, M. and Rollins, A. M. (2011). High-speed optical coherence tomography imaging of the beating avian embryonic heart. *Cold Spring Harb Protoc* **2011**, pdb top98.

Hall, J., Jheon, A. H., Ealba, E. L., Eames, B. F., Butcher, K. D., Mak, S. S., Ladher, R., Alliston, T. and Schneider, R. A. (2014). Evolution of a developmental mechanism: Species-specific regulation of the cell cycle and the timing of events during craniofacial osteogenesis. *Dev Biol* **385**, 380-95.

Hallgrimsson, B., Dorval, C. J., Zelditch, M. L. and German, R. Z. (2004). Craniofacial variability and morphological integration in mice susceptible to cleft lip and palate. *J Anat* **205**, 501-17.

Hamburger, V. and Hamilton, H. (1951). A series of normal stages in the development of the chick embryo. *J. Morphol.* **88**, 49-92.

Hosseini-Farahabadi, S., Geetha-Loganathan, P., Fu, K., Nimmagadda, S., Yang, H. J. and Richman, J. M. (2013). Dual functions for WNT5A during cartilage development and in disease. *Matrix Biol* **32**, 252-64.

Hu, D., Colnot, C. and Marcucio, R. S. (2008). Effect of bone morphogenetic protein signaling on development of the jaw skeleton. *Dev Dyn* **237**, 3727-37.

Jacobs, R. E., Ahrens, E. T., Dickinson, M. E. and Laidlaw, D. (1999). Towards a microMRI atlas of mouse development. *Comput Med Imaging Graph* **23**, 15-24.

Johnston, M. C. and Bronsky, P. T. (1995). Prenatal craniofacial development: new insights on normal and abnormal mechanisms. *Crit Rev Oral Biol Med* **6**, 368-422.

Klingenberg, C. P. (2010). Evolution and development of shape: integrating quantitative approaches. *Nat Rev Genet* **11**, 623-35.

Klingenberg, C. P. (2011). MorphoJ: an integrated software package for geometric morphometrics. *Mol Ecol Resour* **11**, 353-7.

Klingenberg, C. P., Barluenga, M. and Meyer, A. (2002). Shape analysis of symmetric structures: quantifying variation among individuals and asymmetry. *Evolution* **56**, 1909-20.

Klingenberg, C. P. and Monteiro, L. R. (2005). Distances and directions in multidimensional shape spaces: implications for morphometric applications. *Syst Biol* **54**, 678-88.

Landes, C. A., Weichert, F., Geis, P., Helga, F. and Wagner, M. (2006). Evaluation of two 3D virtual computer reconstructions for comparison of cleft lip and palate to normal fetal microanatomy. *Anat Rec A Discov Mol Cell Evol Biol* **288**, 248-62.

Larina, I. M., Baevskii, R. M., Pastushkova, L., Novoselova, N. M., Custaud, M. and Luchitskaia, E. S. (2011). [Seven-day dry immersion: relations between water-electrolyte and cardiovascular responses]. *Fiziol Cheloveka* **37**, 100-7.

Lee, S. H., Bedard, O., Buchtova, M., Fu, K. and Richman, J. M. (2004). A new origin for the maxillary jaw. *Dev Biol* **276**, 207-24.

Li, X., Young, N. M., Tropp, S., Hu, D., Xu, Y., Hallgrimsson, B. and Marcucio, R. S. (2013). Quantification of shape and cell polarity reveals a novel mechanism underlying malformations resulting from related FGF mutations during facial morphogenesis. *Hum Mol Genet* **22**, 5160-72.

Louie, A. Y., Huber, M. M., Ahrens, E. T., Rothbacher, U., Moats, R., Jacobs, R. E., Fraser, S. E. and Meade, T. J. (2000). In vivo visualization of gene expression using magnetic resonance imaging. *Nat Biotechnol* **18**, 321-5.

MacDonald, M. E., Abbott, U. K. and Richman, J. M. (2004). Upper beak truncation in chicken embryos with the cleft primary palate mutation is due to an epithelial defect in the frontonasal mass. *Dev Dyn* **230**, 335-49.

Marcucio, R. S., Young, N. M., Hu, D. and Hallgrimsson, B. (2011). Mechanisms that underlie co-variation of the brain and face. *Genesis* **49**, 177-89.

McGonnell, I. M., Clarke, J. D. and Tickle, C. (1998). Fate map of the developing chick face: analysis of expansion of facial primordia and establishment of the primary palate. *Dev Dyn* **212**, 102-18.

Metscher, B. D. (2011). X-ray microtomographic imaging of intact vertebrate embryos. *Cold Spring Harb Protoc* **2011**, 1462-71.

Metscher, B. D. and Muller, G. B. (2011). MicroCT for molecular imaging: quantitative visualization of complete three-dimensional distributions of gene products in embryonic limbs. *Dev Dyn* **240**, 2301-8.

Minkoff, R. (1984). Cell cycle analysis of facial mesenchyme in the chick embryo. I. Labelled mitoses and continuous labelling studies. *J Embryol Exp Morphol* **81**, 49-59.

Minkoff, R. (1991). Cell proliferation during formation of the embryonic facial primordia. *J Craniofac Genet Dev Biol* **11**, 251-61.

Minkoff, R. and Kuntz, A. J. (1977). Cell proliferation during morphogenetic change; analysis of frontonasal morphogenesis in the chick embryo employing DNA labeling indices. *J Embryol Exp Morphol* **40**, 101-13.

Minkoff, R. and Kuntz, A. J. (1978). Cell proliferation and cell density of mesenchyme in the maxillary process and adjacent regions during facial development in the chick embryo. *J Embryol Exp Morphol* **46**, 65-74.

Minoux, M. and Rijli, F. M. (2010). Molecular mechanisms of cranial neural crest cell migration and patterning in craniofacial development. *Development* **137**, 2605-21.

Mohun, T. J. and Weninger, W. J. (2011). Imaging heart development using high-resolution episcopic microscopy. *Curr Opin Genet Dev* **21**, 573-8.

Muenke, M. and Beachy, P. A. (2000). Genetics of ventral forebrain development and holoprosencephaly. *Curr Opin Genet Dev* **10**, 262-9.

Muenke, M., Solomon, B. D. and Odent, S. (2010). Introduction to the American Journal of Medical Genetics Part C on holoprosencephaly. *Am J Med Genet C Semin Med Genet* **154C**, 1-2.

Ooë, T. (1981). Human Tooth and Dental Arch Development. Tokyo: Ishiyaku Publishers Inc.

Patterson, S. B. and Minkoff, R. (1985). Morphometric and autoradiographic analysis of frontonasal development in the chick embryo. *Anat Rec* **212**, 90-9.

Quintana, L. and Sharpe, J. (2011a). Optical projection tomography of vertebrate embryo development. *Cold Spring Harb Protoc* **2011**, 586-94.

Quintana, L. and Sharpe, J. (2011b). Preparation of mouse embryos for optical projection tomography imaging. *Cold Spring Harb Protoc* **2011**, 664-9.

Radlanski, R. J. (2003). Prenatal craniofacial morphogenesis: four-dimensional visualization of morphogenetic processes. *Orthod Craniofac Res* **6 Suppl 1**, 89-94.

Radlanski, R. J., Renz, H. and Klarkowski, M. C. (2003). Prenatal development of the human mandible. 3D reconstructions, morphometry and bone remodelling pattern, sizes 12-117 mm CRL. *Anat Embryol (Berl)* **207**, 221-32.

Richman, J. M., Buchtova, M. and Boughner, J. C. (2006). Comparative ontogeny and phylogeny of the upper jaw skeleton in amniotes. *Dev Dyn* **235**, 1230-43.

Richman, J. M. and Crosby, Z. (1990). Differential growth of facial primordia in chick embryos: responses of facial mesenchyme to basic fibroblast growth factor (bFGF) and serum in micromass culture. *Development* **109**, 341-8.

Richman, J. M., Herbert, M., Matovinovic, E. and Walin, J. (1997). Effect of fibroblast growth factors on outgrowth of facial mesenchyme. *Dev Biol* **189**, 135-147.

Richman, J. M. and Tickle, C. (1989). Epithelia are interchangeable between facial primordia of chick embryos and morphogenesis is controlled by the mesenchyme. *Dev Biol* **136**, 201-10.

Richman, J. M. and Tickle, C. (1992). Epithelial-mesenchymal interactions in the outgrowth of limb buds and facial primordia in chick embryos. *Dev Biol* **154**, 299-308.

Roessler, E., Belloni, E., Gaudenz, K., Jay, P., Berta, P., Scherer, S. W., Tsui, L. C. and Muenke, M. (1996). Mutations in the human Sonic Hedgehog gene cause holoprosencephaly. *Nat Genet* **14**, 357-60.

Savriama, Y. and Klingenberg, C. P. (2011). Beyond bilateral symmetry: geometric morphometric methods for any type of symmetry. *BMC Evol Biol* **11**, 280.

Schneider, J. E., Bamforth, S. D., Farthing, C. R., Clarke, K., Neubauer, S. and Bhattacharya, S. (2003). High-resolution imaging of normal anatomy, and neural and adrenal malformations in mouse embryos using magnetic resonance microscopy. *J Anat* **202**, 239-47.

Schneider, R. A. and Helms, J. A. (2003). The cellular and molecular origins of beak morphology. *Science* **299**, 565-8.

Sharpe, J. (2003). Optical projection tomography as a new tool for studying embryo anatomy. *J Anat* **202**, 175-81.

Sharpe, J. (2004). Optical projection tomography. *Annu Rev Biomed Eng* **6**, 209-28.

Sharpe, J., Ahlgren, U., Perry, P., Hill, B., Ross, A., Hecksher-Sorensen, J., Baldock, R. and Davidson, D. (2002). Optical projection tomography as a tool for 3D microscopy and gene expression studies. *Science* **296**, 541-5.

Shuler, C. F. (1995). Programmed cell death and cell transformation in craniofacial development. *Crit Rev Oral Biol Med* **6**, 202-17.

Stiebel-Kalish, H., Weinberger, D., Barash, D. and Yassur, Y. (1997). [Ultrasound biomicroscopy--microscopic resolution imaging]. *Harefuah* **133**, 570-3.

Sun, D., Baur, S. and Hay, E. D. (2000). Epithelial-mesenchymal transformation is the mechanism for fusion of the craniofacial primordia involved in morphogenesis of the chicken lip. *Dev Biol* **228**, 337-49.

Szabo-Rogers, H. L., Geetha-Loganathan, P., Nimmagadda, S., Fu, K. K. and Richman, J. M. (2008). FGF signals from the nasal pit are necessary for normal facial morphogenesis. *Dev Biol* **318**, 289-302.

Szabo-Rogers, H. L., Geetha-Loganathan, P., Whiting, C. J., Nimmagadda, S., Fu, K. and Richman, J. M. (2009). Novel skeletogenic patterning roles for the olfactory pit. *Development* **136**, 219-29.

Thompson, D. A. W. (1917). On growth and form. Cambridge: University Press.

Thompson, H., Griffiths, J.S., Jeffery, G., and McGonnell, I.M. (2010). The retinal pigment epithelium of the eye regulates the development of scleral cartilage. *Dev Biol* **347,** 40-52.

van Raaij, M. E., Lindvere, L., Dorr, A., He, J., Sahota, B., Foster, F. S. and Stefanovic, B. (2011). Functional micro-ultrasound imaging of rodent cerebral hemodynamics. *Neuroimage* **58**, 100-8.

Vermeij-Keers, C., Poelmann, R. E., Smits-Van Prooije, A. E. and Van der Meulen, J. C. (1984). Hypertelorism and the median cleft face syndrome. An embryological analysis. *Ophthalmic Paediatr Genet* **4**, 97-105.

Wallingford, J. B., Fraser, S. E. and Harland, R. M. (2002). Convergent extension: the molecular control of polarized cell movement during embryonic development. *Dev Cell* **2**, 695-706.

Walls, J. R., Sled, J. G., Sharpe, J. and Henkelman, R. M. (2005). Correction of artefacts in optical projection tomography. *Phys Med Biol* **50**, 4645-65.

Wedden, S. E. (1987). Epithelial-mesenchymal interactions in the development of chick facial primordia and the target of retinoid action. *Development* **99**, 341-51.

Weninger, W. J. and Mohun, T. (2002). Phenotyping transgenic embryos: a rapid 3-D screening method based on episcopic fluorescence image capturing. *Nat Genet* **30**, 59-65.

Wu, P., Jiang, T. X., Shen, J. Y., Widelitz, R. B. and Chuong, C. M. (2006). Morphoregulation of avian beaks: comparative mapping of growth zone activities and morphological evolution. *Dev Dyn* **235**, 1400-12.

Wu, P., Jiang, T. X., Suksaweang, S., Widelitz, R. B. and Chuong, C. M. (2004). Molecular shaping of the beak. *Science* **305**, 1465-6.

Young, N. M., Chong, H. J., Hu, D., Hallgrimsson, B. and Marcucio, R. S. (2010). Quantitative analyses link modulation of sonic hedgehog signaling to continuous variation in facial growth and shape. *Development* **137**, 3405-9.

Young, N. M., Hu, D., Lainoff, A. J., Smith, F. J., Diaz, R., Tucker, A. S., Trainor, P. A., Schneider, R. A., Hallgrimsson, B. and Marcucio, R. S. (2014). Embryonic bauplans and the developmental origins of facial diversity and constraint. *Development* **141**, 1059-63.

Young, N. M., Wat, S., Diewert, V. M., Browder, L. W. and Hallgrimsson, B. (2007). Comparative morphometrics of embryonic facial morphogenesis: implications for cleft-lip etiology. *Anat Rec (Hoboken)* **290**, 123-39.

Zelditch, M., Swiderski, D. and Sheets, H. D. (2012). Geometric morphometrics for biologists : a primer. Amsterdam ; London: Elsevierc.